Collective scattering on the TORTUR tokamak

Sips, A.C.C.

Award date:
1987

COLLECTIVE SCATTERING ON THE TORTUR TOKAMAK

A.C.C. Sips

I.R. 87/056

COLLECTIVE SCATTERING

ON THE

TORTUR TOKAMAK

by

A.C.C. Sips

Afstudeerdocent: Prof. DR. L.Th.M Ornstein

Begeleiding: Ir. G.J.J. Remkes

November, 1987

FOM Instituut voor Plasmafysica "Rijnhuizen", Nieuwegein.

Abstract

Density fluctuations in the TORTUR plasma are observed by 2 mm wave scattering.
The frequency shift of the scattered radiation due to the scattering process could be determined at various wavenumbers of the fluctuations.
A theory on the wavenumber resolution and the observed fluctuation level within this resolution is given. The required power for the microwave source could be calculated assuming that power of the scattered radiation must exceed the power of the electron cyclotron radiation that can be detected (emission near the second harmonic frequency).
A lens system is developed to shape the microwave beam which is injected into the plasma. Power losses in the beam transport system and in the TORTUR tokamak and could be measured. These power losses are minimized.
The first results showed that the frequencies of the density fluctuation lied within the range of 10 kHz to 500 kHz.
A rapid change (within 25 μs) of the total power of the scattered signal has been observed.

Contents

Chapter 1: Introduction

1.1: TORTUR

The TORTUR device at the FOM Institute for Plasma Physics at Nieuwegein is a toroidal plasma confinement system of the tokamak type.
The hydrogen plasma is produced in the toroidal chamber by inducing an electrical discharge. Several capacitor banks feed a transformer to induce the plasma current. A set of coils around the vacuum chamber generate a toroidal magnetic field. The poloidal field resulting from the plasma current in combination with the toroidal magnetic field yield the typical helical field configuration of a tokamak, ensuring confinement of the charged particles. Finally, a vertical magnetic field stabilizes the position of the plasma column.

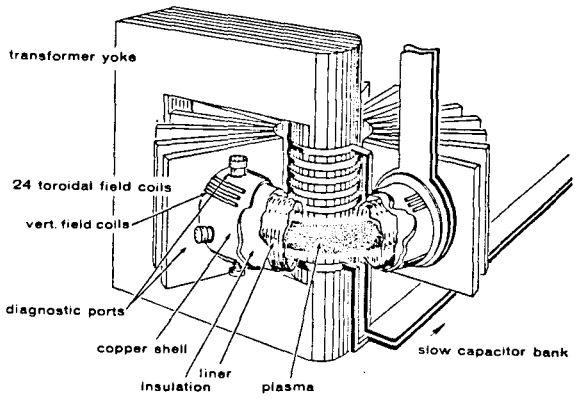

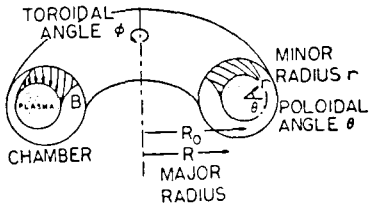

Figure 1: Tortur, a schematic drawing.

table 1: Machine parameters

Major radius:	R_0	= 0.46 m.
Radius of the copper shield:	r_s	= 0.105 m.
Limiter radius:	a_l	= 0.080 m.
Magnetic field:	B_0	= 2.9 Tesla
Plasma volume:	Vol	= 0.06 m^3

A discharge is started using a 200 Watt r.f. signal to ionize the hydrogen gas. A fast capacitor bank is used for a rapid energy input

into the plasma. This plasma formation stage is characterized by a steep rize of the plasma current. A second bank takes over the discharge after a few milliseconds and maintains the current for about 30 milliseconds. The characteristics of a TORTUR discharge are given in table 2 and figure 2.

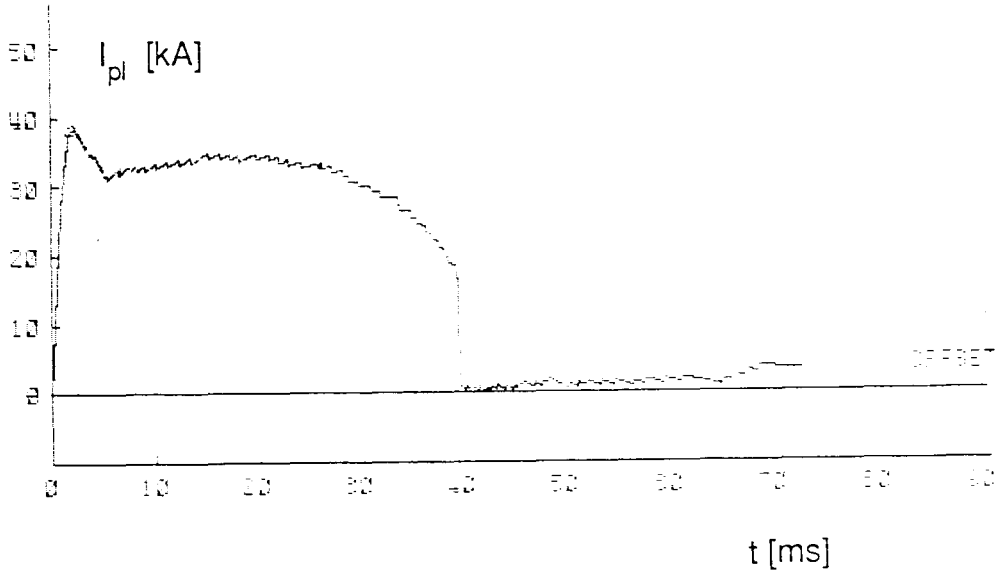

Figure 2: Plasma current versus time.

Table 2: Main plasma parameters

Plasma current:	I_p = 35 kA.	
Loop voltage:	V_l = 4-5 V.	
Electron temperature:	T_e = 700 eV	(at r = 5 mm.)
Ion temperature:	T_i = 400 eV	(at r = 5 mm.)
Electron density:	$n_e = 6*10^{19}$ m^{-3}	(at r = 5 mm.)

The purpose of the TORTUR experiment is to study anomalous plasma heating by enhancing the ohmic dissipation of the plasma current. For this purpose the device is equiped with a high voltage capacitor bank which can be fired at any preset time during the plateau stage of the discharge to give an I-plasma spike up to 60 kA.
This pulse excites micro instabilities which cause a larger resistance and as a result of that the desired anomalous heating may occure (turbulent heating).

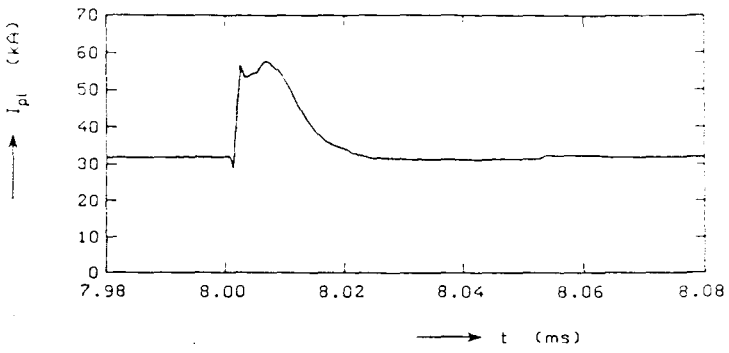

Figure 3: The current pulse on the plateau of I-plasma.

It has become clear during recent years of experimentation that the device can produce two types of discharges, namely a discharge with a high loop voltage (4-5 V) and a low one (1-2 V). The high loop voltage type is weakly turbulent and has already an enhanced ohmic dissipation.
Investigation of the differences between the two discharges will be the goal of the next series of experiments.

1.2: Diagnostics on TORTUR

In order to get information about the physical processes in the plasma and the plasma properties as shown in table 2 and figure 2, several diagnostic tools are used.
These diagnostics are:

- Rogowski coils to determine the plasma current.
- A loop voltage divider to give the loop voltage of the discharge.
- A sinus-cosinus coil set to record the vertical and horizontal plasma position.
- A bolometer to measure the power loss to the wall of the toroidal chamber.
- A Thomson-scattering device to determine the electron density and temperature at two radial positions (only one radial position can be measured at a plasma shot).
- An electron cyclotron emission polychromator to measure time resolved radial electron temperature profiles and non-thermal electron populations.
- A time of flight analyser to give the velocity distribution of low energy neutrals from the outer plasma region.

- An eight-channel electrostatic analyser to determine the neutral particle flux out of the plasma. Together with an active neutral beam probe it gives the central ion temperature.
- Visible light and U.V. polychromators to measure the line spectra emitted by the impurities, thus giving indication of the concentrations of the impurities and their states of ionization.
- A four-channel soft X-ray detector to record the X-ray flux, to monitor the electron temperature and to determine Z_{eff}.
- A collective scattering device to analyse the density fluctuations.

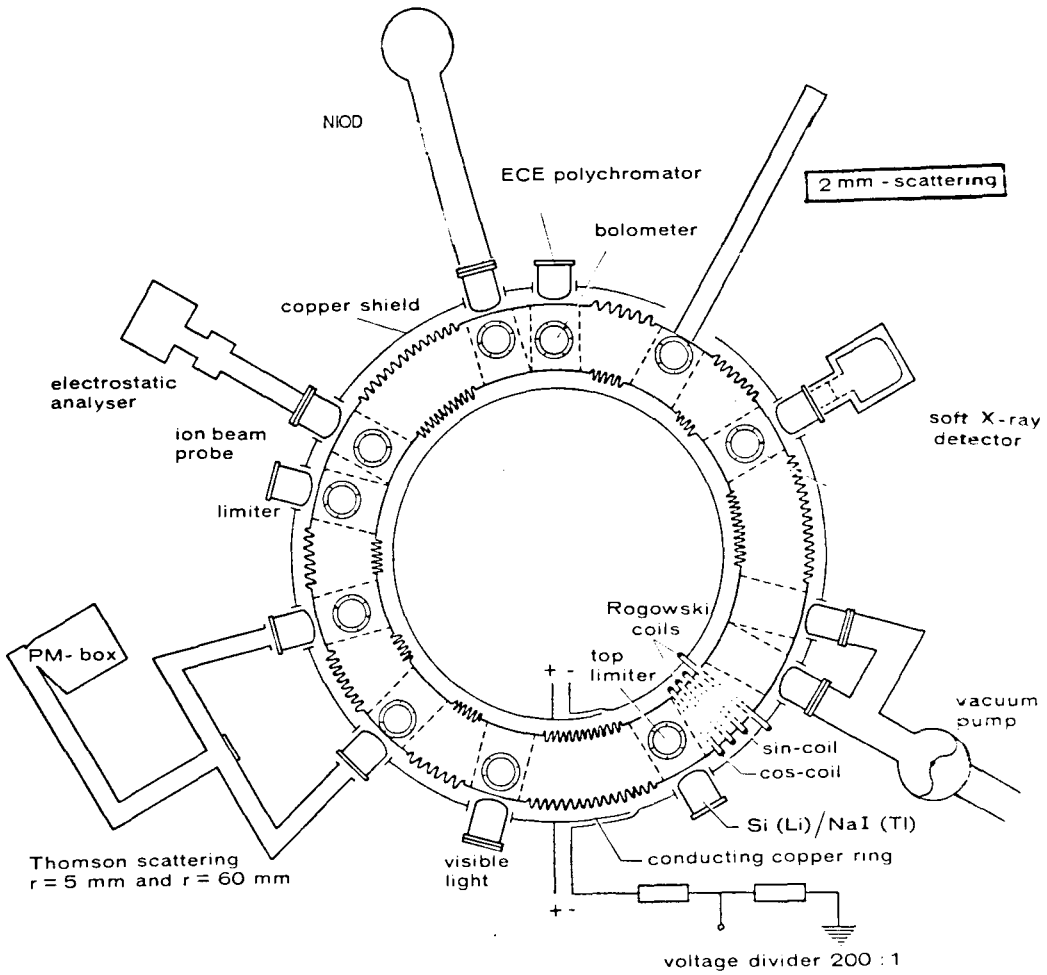

Figure 4: The diagnostic equipment of TORTUR.

1.3: Collective scattering as a diagnostic tool

Density fluctuations in a tokamak plasma may give rize to enhanced particle and thermal transport across the confining magnetic field. [1,2]
The analysis of the fluctuations by means of collective scattering is of great importance in fusion research [3].
The wavelengths used to perform collective scattering vary from infrared to the microwave region of the electromagnetic spectrum depending on the plasma size and density, port access, and range of wavevectors to be resolved.
In most cases the scattering process takes place within the poloidal plane of the torus. The incident beam is injected into the plasma (perpendicularly to plasma current) and is scattered by density fluctuations with different wavenumbers $\underline{k}$. The scattering angles depend on these wavevectors and on the wavelength of the incident beam.
Since 1982 ninety degree scattering of 4 mm waves has been performed on TORTUR at the plasma edge [6,7].
This report discusses the development of a 2 mm scattering diagnostic which can be used to study the scattered radiation in the angle regions of 5^{o} to 50^{o} and 90^{o} to 115^{o}. The apparatus has the possibility to give a spatial map of the fluctuations.
Chapter 2 discusses the Gaussian beam theory, followed by theory on the scattering condition, wave vector resolution and a calculation of the source power needed to perform the experiment. The theory is used to develop the diagnostic system (chapter 3).
The first, preliminairy experimental results are given in chapter 4.

Chapter 2: Theory

Collective scattering can be understood as an interaction between electromagnetic waves and electron density waves.
The intensity distribution of the 2 mm. probing beam is Gaussian and is not changed by the scattering process.
This Gaussian distribution is used to define the radius of the beam. The spatial resolution and the resolution of the wavevectors of the density fluctuations ($\underline{k}$-resolution) depend on this radius. The expressions that will be derived are valid for scattering angles between 5° - 50° and 90° - 115°. In literature small angle approximations, relating to CO_2 laser scattering (λ=10.3μm), are given. The relations found and the differences between large and small angle scattering will be discussed in secton 2.3.

2.1: The scattering condition

The electron density waves (fluctuations) have a frequency ω and wavenumber $\underline{k}$.
If the incident beam (ω_0 , $\underline{k}_0$) is scattered by the fluctuations it must satisfy momentum and energy conservation requirements so that

$$\omega_s = \omega_0 \pm \omega \qquad \text{and} \qquad \underline{k}_s = \underline{k}_0 + \underline{k} \qquad (1)$$

Where ω_s : Frequency of the scattered radiation.

$\underline{k}_s$: Wavevector of the scattered radiation.

For wavenumbers of interest (k = 1-50 cm^{-1}) the magnitude of the incident and scattered wave vectors are approximately equal ($|k_0| \approx |k_s|$) thereby yielding

$$k = 2 k_0 \sin\left(\frac{\theta_s}{2}\right) \qquad (2)$$

where θ_s = scattering angle

and $k_0 = \frac{2\pi}{\lambda_0}$

This relation is the scattering condition and equals the familiar Bragg relation.
One can see that in the case of 2 mm. scattering and density wave vectors of interest θ_s will be large and in the case of CO_2 laser scattering θ_s will be a few millirads.
The frequency shifted radiation (Eq. (1)) is mixed with that of a reference beam (local oscillator) in a reciever. This results in a signal with an amplitude which is proportional to the electric field amplitude of the scattered beam. The frequency shift of the scattered radiation can be determined. If the frequencies of the local oscillator and probing beam are equal the mixing technique is homodyne.

2.2: Gaussian beam theory

The 2-mm. beam that will be scattered in the plasma is produced by a 140 GHz klystron which is connected to a waveguide system (see next chapter).
The electric field component ϕ of a wave, propagating in free space, can be given by

$$\phi = u(x',y',z')\, e^{-ikz'} \qquad (3)$$

where z' is the direction of propagation and u(x',y',z') represents the difference between the Gaussian beam and a plane wave.
Inserting Eq. (3) into the wave equation yields a solution which can be written as a product of a Hermite polynome, a Gaussian transverse amplitude variation and a phase factor. The set of Hermite polynomials can be identified with the modes of propagation of the radiation. Only the fundamental mode will be discussed here.
The Gaussian transverse amplitude variation determines the

intensity distribution of the wave

$$I(r,t) = I_0(t)\,\exp\left(\frac{-2r^2}{w^2}\right) \qquad (4)$$

The beam radius w equals the half width at the 1/e point of the E-field profile.

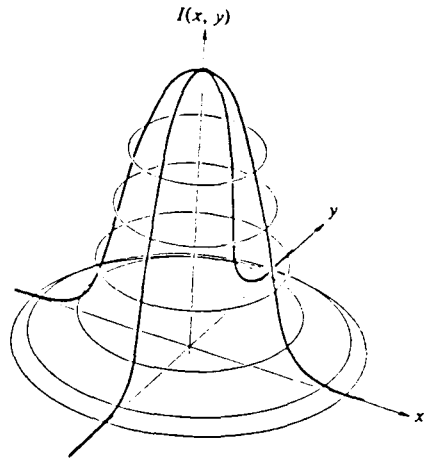

Figure 5: The Gaussian intensity distribution

The Gaussian beam contracts to a minimum radius w_0 at the so called beam waist where the phase front is plane.
The expansion of the radius along the axis of propagation is given by

$$w(z') = \sqrt{w_0^2 + \left(\frac{\lambda z'}{\pi w_0}\right)^2} \qquad (5)$$

when the beam waist is located at z' = 0.
From Eq. (5) follows the assymtotic growth in angle of the beam radius (divergence angle)

$$\theta\,[\text{degrees}] = \left(\frac{\lambda\,[\text{mm}]}{\pi w_0\,[\text{mm}]}\right)\left(\frac{360}{2\pi}\right) \qquad (6)$$

Finally, the radius of curvature R of the phase front is defined as

$$R(z') \equiv z'\left(1 + \left(\frac{\pi w_0^2}{\lambda z'}\right)^2\right) \qquad (7)$$

The propagation of a Gaussian beam in the vicinity of its waist is shown in Fig. 8.

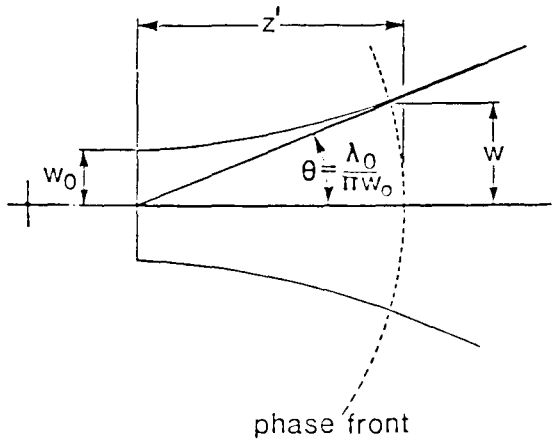

Figure 6: Contour of a Gaussian beam.

Focussing of a Gaussian beam:

A lens will be used to adjust the microwave beam to the dimensions of a given structure and to achieve a well defined spatial resolution. An ideal thin lens of focal length f transforms the radius of curvature R_1 of the phase front, to the left of the lens, into R_2 immediately to the right of it

$$\frac{1}{R_2} = \frac{1}{R_1} - \frac{1}{f} \qquad (8)$$

The diameter of the beam at the position of the lens (z_{lens}) is not changed by the presense of the lens. Using this and Eq.(8) the position z_{waist} and the radius w_{waist} of the new formed waist can be found [15]

$$\frac{1}{w_{waist}^2} = \frac{1}{w_0^2}\left(1 - \frac{z_{lens}}{f}\right)^2 + \frac{1}{f^2}\left(\frac{\pi w_0}{\lambda}\right)^2 \qquad (9)$$

$$z_{waist} = f - \frac{(z_{lens} - f) f^2}{\left((z_{lens} - f)^2 + \left(\frac{\pi w_0^2}{\lambda}\right)^2\right)} \qquad (10)$$

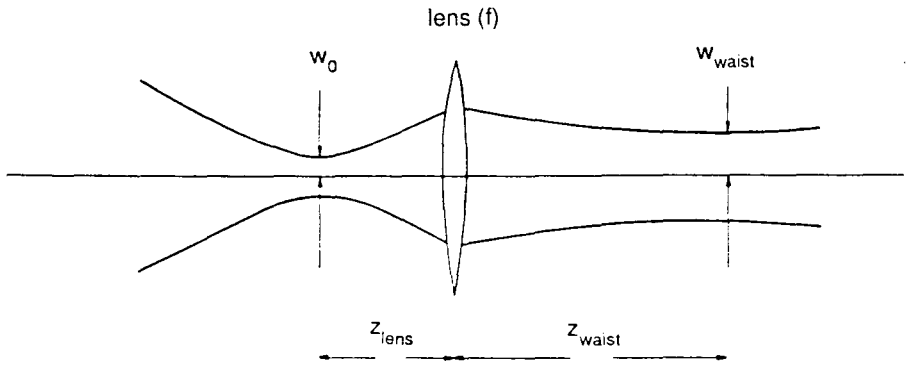

Figure 7: A lens in the Gaussian beam

Power transport:

The microwave beam must pass several components (lenses, diagnostic windows of TORTUR) which truncate the beam and reduce the total transmitted power.
The equations found can be used to define a criterium for the optimal power transmission of the truncating components. The total transported power by the microwave beam is given by a proper integration of Eq. (4).

$$P_{total} = 2\pi < I_0(t) > \int_0^{\infty} r \exp\left(\frac{-2r^2}{w^2}\right) dr = \frac{1}{4}\pi I_0 w^2 \qquad (11)$$

The transmitted power through a circular element of radius R_{eff} is

given by

$$P_{transm.} = 2\pi < I_0(t) > \int_0^{R_{eff}} r \exp\left(\frac{-2r^2}{w^2}\right) dr = \tag{12}$$

$$= \frac{1}{4}\pi I_0 w^2 \left(1 - \exp\left(\frac{-2R_{eff}^2}{w^2}\right)\right)$$

While the transmissivity of the element equals the ratio of Eq. (11) and (12).

$$T = 1 - \exp\left(\frac{-2R_{eff}^2}{w^2}\right) \tag{13}$$

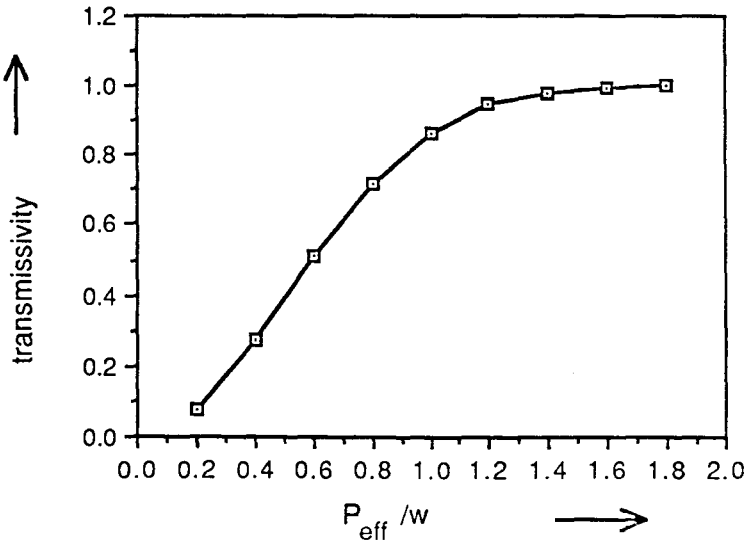

Figure 8: The transmissivity as a function of R_{eff} / w

Since w is a quadratic function of the distance z' from the waist an optimum radius (w_{opt}) can be found at the truncating element, by differentiating Eq. (5) with respect to w_0, yielding

$$w_{opt} = \sqrt{\frac{2\lambda z_0}{\pi}} \qquad (14)$$

$$w_0 = \sqrt{\frac{\lambda z_0}{\pi}} \qquad (15)$$

Where z_0 is the distance of the waist to the truncating element.
So when the waist position is known the optimal w_0 can be calculated. The final choice of the waist radius depends on the distance from the most critical truncating component of the experimental set up.
The equations found in this section will be used to adjust the microwave beam to the torus structure (see chapter 3).

2.3: k-resolution, fluctuation level and minimum source power required to perform the scattering experiment.

The scattered radiation can only be studied at a certain angle, giving a scattered 'beam' which is recieved and and detected. The dimensions of this scattered beam are approximately equal to the dimensions of incident beam. The two beams intersect at the position where the fluctuation are studied yielding a volume where the scattering process takes place. The extension of the observed volume defines the spatial resolution.

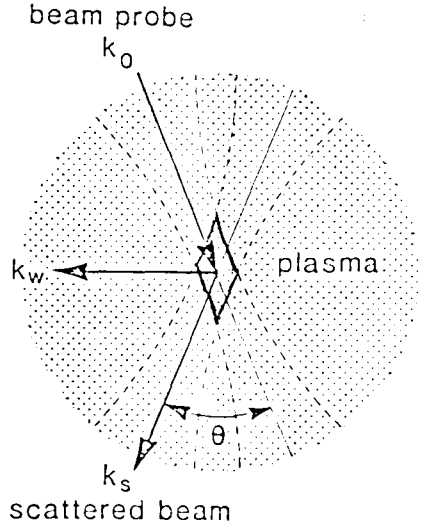

Figure 9: The scattered and incident beam.

The observed volume V is determined by the beam radii of both incident and scattered beam and by the scattering angle. Since the Gaussian distribution defines the beam radius it plays an important role in the definition of the spatial resolution.
The $\underline{k}$-resolution is coupled to the spatial resolution by means of a Fourier transform. Because of this a small observed volume V implies a bad $\underline{k}$-resolution.
The use of a CO_2 laser to perform the experiment causes small scatering angles which result in a length L_V of the observation volume (in the direction of the propagation of the laser beam) larger than the plasma radius [5]. In case of 2 mm. waves both spatial and $\underline{k}$-resolution are acceptable. Also the problems of distinguishing the scattered beam from the incident beam may occur when a CO_2 laser is used.

A special coordinate grid is used to derive the expressions for the observed volume and the $\underline{k}$-resolution [4]. The angle between the z axis and the propagation direction (in section 2.2 the z' axis) of both incident and scattered beam is equal to the half of the scattering angle.

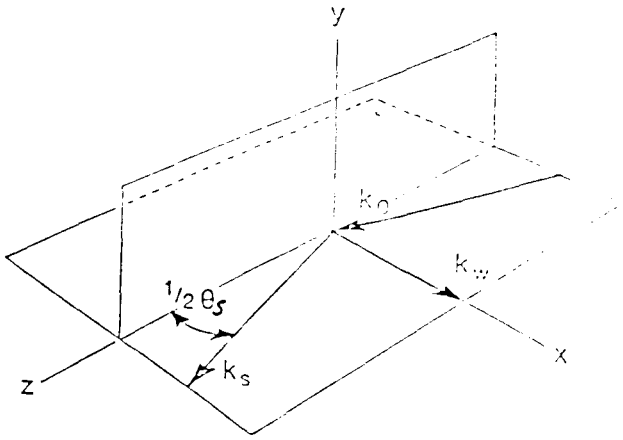

Figure 10: The coordinate grid.

Expressing the Gaussian profile in the coordinate grid of the scattering process gives the following transverse electric field distributions [4]

$$u_{incident}(r) = \exp\left\{ \frac{-1}{w^2} \left[y^2 + \left(x + z \tan\left(\frac{\theta_s}{2}\right)\right)^2 \right] \cos^2\left(\frac{\theta_s}{2}\right) \right\} \quad (16)$$

$$u_{scattered}(r) = \exp\left\{ \frac{-1}{w^2} \left[y^2 + \left(x - z \tan\left(\frac{\theta_s}{2}\right)\right)^2 \right] \cos^2\left(\frac{\theta_s}{2}\right) \right\}$$

The signal from the scattering process is proportional to the product $u_{incident}^{*} u_{scattered}$, which is the space response function U(r), it defines the observed volume V

$$V \equiv \int U^2(r)\, dr = \frac{\pi^{3/2} w_0^3}{4 \sin\theta_s} \quad (17)$$

The spatial resolution in one direction may be defined as the half width of $U^2(r)$ at the 1/e value.
The k-space weighting function can be found by Fourier transformation of U(r) which gives.

$$W(k) = \frac{2\left(\frac{\pi}{2}\right)^{3/2} w_0^3}{\sin\theta_s} \exp\left\{ \frac{-w_0^2}{8} \left[k_y^2 + \left(k_x^2 + k_z^2 \tan^{-2}\left(\frac{\theta_s}{2}\right)\right) \cos^{-2}\left(\frac{\theta_s}{2}\right) \right] \right\} \quad (18)$$

The one dimensional k-resolutions are found from the half width of $W^2(k)$ at the 1/e value

$$\Delta k_x = \frac{2}{w_0} \cos\left(\frac{\theta_s}{2}\right) \quad (19)$$

$$\Delta k_y = \frac{2}{w_0} \quad (20)$$

$$\Delta k_z = \frac{2}{w_0} \sin\left(\frac{\theta_s}{2}\right) \quad (21)$$

yielding

$$\Delta k^3 = \frac{4}{w_0^3} \sin\theta_s \qquad (22)$$

Within the resolutions found the density fluctuations are observed. The time varying part of the density is

$$\tilde{n}(\underline{r},t) = n(\underline{r},t) - \bar{n}(\underline{r}) \qquad (23)$$

$$\text{with} \qquad \bar{n} = \lim_{T\uparrow\infty} \int^{T} n(\underline{r},t)\,dt$$

In practice T > (discharge time) is regarded as infinite. Since the observed fluctuations are modulated by the space response function $U(\underline{r})$, the weighted mean square is

$$\langle \tilde{n}^2 \rangle_{uT} = \frac{\int^{T} dt \int \tilde{n}^2(\underline{r},t)\,|U(\underline{r})|^2\,d\underline{r}}{T\int |U(\underline{r})|^2\,d\underline{r}} \qquad (24)$$

Fourier transforming this in space and time and performing some straightforeward calculations the following expression is found [9].

$$\langle \tilde{n}^2 \rangle_{uT} = \int \frac{d\underline{k}}{\Delta k^3} \langle \tilde{n}^2 \rangle_{kr} \qquad (25)$$

$$\text{where} \qquad \langle \tilde{n}^2 \rangle_{kr} = \frac{1}{TV} \frac{\Delta k^3}{(2\pi)^3} \int \frac{(\tilde{n}(\omega)U)_k^2}{2\pi}\,d\omega \qquad (26)$$

An expression for the current in the detector i_k (t) caused by mixing the scattered radiation with that of the local oscillator is

derived in literature [5]. Using this and the Gaussian beam relations one can find [9]

$$< \tilde{n}^2 >_{kr} = \frac{< i_k^2 (t) >}{4 \pi^3 V \alpha} \Delta k^3 \qquad (27)$$

$$\alpha = \frac{16 \lambda_0^2}{\pi^2 w_0^4} \frac{d \sigma_T}{d \Omega} P_s P_{lo} \left(\frac{e \eta}{\hbar \omega_0}\right)^2 \qquad (28)$$

where $\left(\frac{d \sigma_T}{d \Omega}\right)$: Thomson cross-section

P_s , P_{lo} : Source and local oscillator power

η : Detector efficiency

Since $< \tilde{n}^2 >_{Kr}$ is now expressed in known quantities only

$< \tilde{n}^2 >_{UT}$ can be calculated by integrating over k - space.
Approximating this intergration by a summation using a uniform k distribution [9] one arrives at

$$< \tilde{n}^2 >_{uT} = \beta \sum_i \frac{k_i^2 < i_{k_i} (t) >}{4 \pi^{5/2} \lambda_0^2 \left(\frac{d \sigma_T}{d \Omega}\right) P_0 P_{lo}} \frac{\sin^2 \theta_{s_i}}{\sin \left(\frac{\theta_{s_i}}{2}\right)} \left(\frac{\hbar \omega_0}{e \eta}\right)^2$$

(29)

With P_0 : The power of the incident beam at the observed volume

and β : A constant which equals $(dk/\Delta k_x)$

Minimum source power needed:

At a fixed scattering angle and wavelength the only variable quantities in Eq. (29) are P_0 and P_{lo}. Since one source is used to perform the experiment the following expression is valid

$$P_{source} = \frac{1}{T_{br}} \left(\frac{P_{lo}}{T_{lo}} + \frac{P_0}{T_{pl}} \right) \qquad (30)$$

With T_{br} : The transmission of the element which branches off the local oscillator.

T_{lo} : Transmission of the local oscillator branch.

T_{pl} : Transmission of the branch of the incident beam and the recieving branch.

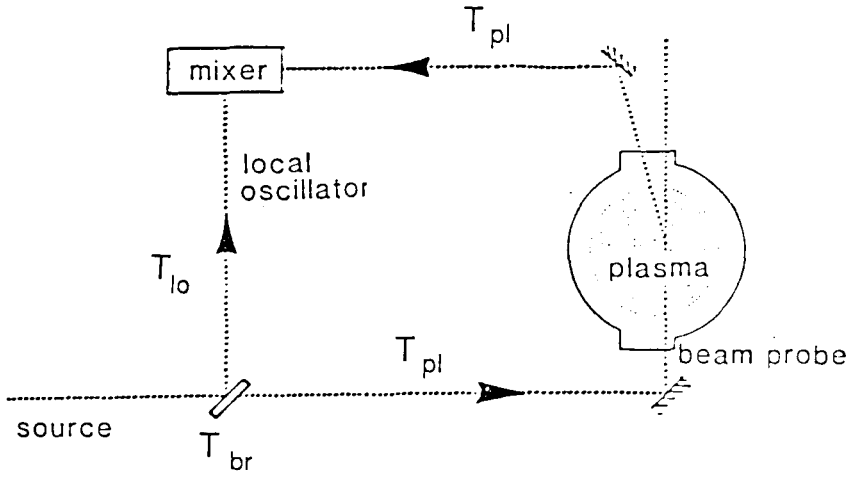

Figure 11: The transmission factors.

The minimum source power required to perform the scattering experiment follows from the noise power in the recieving mixer (Alpha, type: 9608F02HR). The power of the scattered radiation must at least equal this noise power.
There are two major noise factors:

- (Noise equivelent power) * (bandwidth of the detection and recording system) = NEP*B.
  NEP = 4 10^{-20} W/Hz for the Alpha mixer.
  Measurements done with the 4 mm scattering apparatus and the measurements on the TEXT tokamak [3] show that the dominant part of the frequency shift of the scattered signal lies within 2 MHz. So B will be 2MHz.
- The plasma electron cyclotron emission near the second harmonic frequency [10].

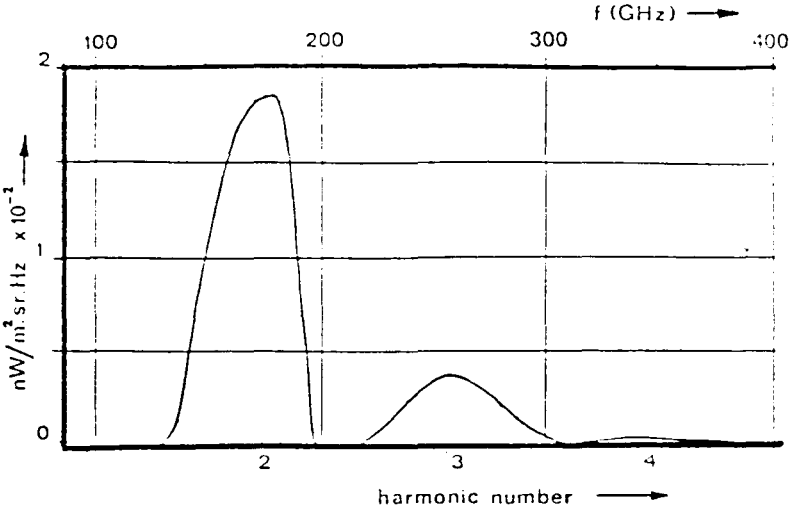

Figure 12: E.C.E spectrum in TORTUR (plasma conditions: see table 2). The fundamental frequency (85 GHz) is not shown here.

The E.C.E power $I_{ece}\,\lambda_o^2\,B$ recieved in the recieving branch, with transmission factor T_{pl} will be mixed with that of the local oscillator which result in the following power in the mixer

$$P_{noise,\,ece} = L\,P_{lo}\,(I_{ece}\,\lambda_0^2\,B)\,T_{pl} \qquad (31)$$

where L is the conversion efficiency of the mixer.
So the total noise in the detector will be

$$P_{noise,\,total} = (NEP + L\,P_{lo}\,I_{ece}\,\lambda_0^2\,T_{pl})\,B \qquad (32)$$

Equation (27) can be rewritten using Eqs. (17),(22), and (28) yielding

$$\langle \tilde{n}^2 \rangle_{kr} = \frac{\sin^2\theta_s}{4\,\pi^{5/2}\,(\frac{d\,\sigma_T}{d\,\Omega})\,w_0^2\,\lambda_0^2}\;\frac{R_d\,\langle i_k^2(t)\rangle}{L P_0\,P_{lo}} \qquad (33)$$

where R_d : The detector resistance

and using $L \equiv \left(\frac{e\,\eta}{\hbar\,\omega_0} \right)^2 R_d$

$R_d < i_k^2(t) >$ is the power in the mixer due to the scattering proces. Taking into account the transmission of the recieving branch and the requirement that the signal to noise ratio N must be larger than or equal to one, it is obvious that

$$R_d < i_k^2(t) > \geq \frac{1}{T_{pl}} P_{noise,\,total} \qquad (34)$$

The choice of the minimum value of $< \tilde{n}^2 >_{kr}$ is based on the results of 4 mm. scattering [8] and is used to determine P_0 as a function of P_{lo}. The minimum fluctuation level we want to detect is:

$$\frac{\tilde{n}}{n_e} = 10^{-5}$$

At the plasma centre the density lies between $2\ 10^{19}\ m^{-3}$ and $6\ 10^{19}\ m^{-3}$.

$$< \tilde{n}^2 >_{kr,\,minimum} = 4\ 10^{28}\ m^{-6}$$

$$\frac{d\,\sigma_T}{d\,\Omega} = 8\ 10^{-30}\ m^2$$

$$L = 20\ W^{-1}$$

$$P_0 = \frac{0.76}{\lambda_0\,[\,mm.\,]\,P_{lo}\,[\,mW.\,]} \frac{N}{T_{pl}} \left(1 + \frac{L\,P_{lo}\,[\,mW.\,]\,\lambda_0^2\,[\,mm^2\,]\,T_{pl}\,I_{ece}}{NEP\ 10^9} \right)$$

(35)

The dependency of θ_s and w_0 on λ_0 is used to achieve this result; the equations (2) (scattering condition) and (15) (optimal waist radius) give these dependencies.
Inserting Eq. (35) into Eq. (30) yields

$$P_{source} = \frac{1}{T_{br}} \left\{ \frac{P_{lo}}{T_{lo}} + \frac{0.76\ N}{\lambda_0\ P_{lo}\ T_{pl}^2} \left[1 + \frac{L\ T_{pl}\ P_{lo}\ \lambda_0^2\ I_{ece}}{NEP\ 10^9} \right] \right\} \qquad (36)$$

This equation can be minimized by differenciating with respect to P_{lo} giving an optimal local oscillator power in the mixer.

$$P_{lo,\,optimal} = \sqrt{\frac{0.76\ N\ T_{lo}}{\lambda_0\ T_{pl}^2}} \qquad (37)$$

Tabel 3 uses the following transmission factors (see section 3.3)

$$T_{br} = 0.8$$
$$T_{lo} = 0.75$$
$$T_{pl} = 0.3$$

Tabel 3:

N	$P_{lo,\,opt}$	$P_{source,\,minimal}$	I_{ece} [W/m^{2}srHz]
1	1.72 mW.	73.5 mW.	$2\ 10^{-11}$ (max.)
1	1.72 mW.	22.7 mW	$5\ 10^{-12}$
1	1.72 mW	5.7 mW	0
2	2.43 mW	143.6 mW	$2\ 10^{-11}$
2	2.43 mW	42.0 mW	$5\ 10^{-12}$
2	2.43 mW	8.1 mW	0
3	2.98 mW	213.2 mW	$2\ 10^{-11}$
3	2.98 mW	60.8 mW	$5\ 10^{-12}$
3	2.98 mW	9.9 mW	0

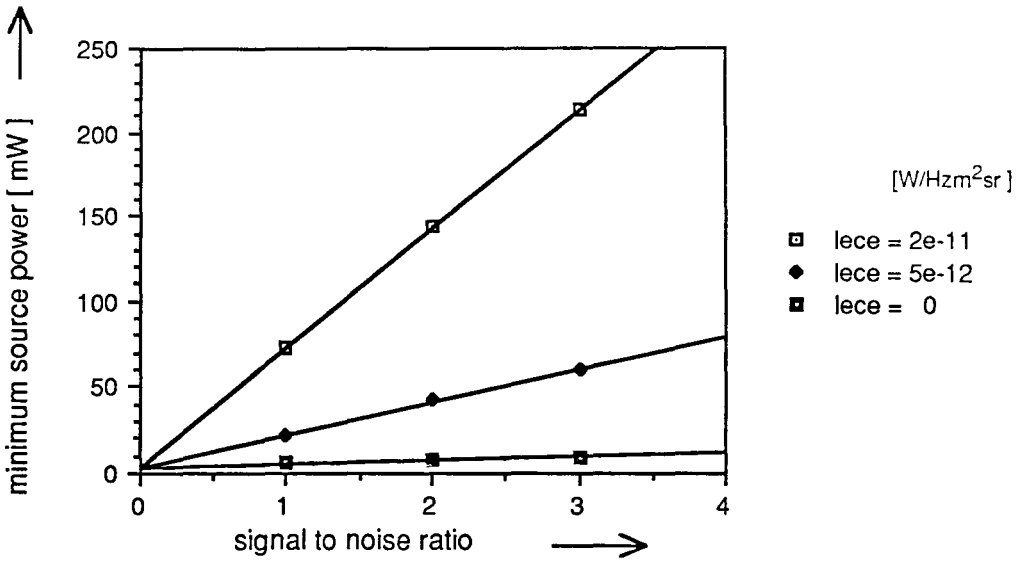

Figure 13: T The minimum source power needed to detect the minimum fluctuation level as a function of the signal to noise ratio. The noise power is calculated for three different values of I_{ece} near the second harmonic frequency.

One can see that the required source power is dominated by the total amount of E.C.E plasma light which is a strong function of the plasma characteristics. Because of this, the signal to noise ratio N varies with the magnetic field, density, and electron temperature of the plasma.
In a one channel set-up several plasma shots are needed to investigate different k-values. These plamsa shots must be the same, otherwize the signal to noise ratio will be different at each k value.
The only way to avoid these problems is to build a multi-channel system which investigates several wave vectors at one instant in time.
Another important factor is the transmission of the incident beam branch and recieving branch, special care must be taken to avoid large power loss in the microwave beam transport (see chapter 3).

2.4: Density fluctuations

Density fluctuation with a small spatial space compared to the

minor radius of the torus are called micro instabilities.
These micro instabilities have been observed by 4 mm scattering at the plasma edge. The dominant part of the scattered radiation, measured at a wavenumber of 17 cm^{-1}, had a frequency shift of 10 kHz to 500 kHz.
The density fluctuations in this frequency domain where attributed to electrostatic, universal drift waves [6,7,13].
These drift waves are induced by a pressure gradient in the plasma.
The appendix gives a derivation of the dispersion equation which describes the characteristics of universal drift waves.
The real part of the solution $\omega = \omega_r + i\gamma$ of this dispersion equation relates

$$\frac{\omega_e^*}{\omega_r} = \frac{\frac{T_e}{T_i}\,(1 - \exp(-b_i)\, I_0(b_i)) + 1}{\exp(-b_i)\, I_0(b_i)} \qquad (38)$$

Where $b_i = k_y \rho_i$ (ρ_i : Ion larmor radius).

I_0 = modified Bessel funtion.

ω_e^* = the electron drift frequency which is given by

$$\omega_e^* \equiv k_y [m^{-1}] \left(\frac{1}{n}\frac{dn}{dx}\right) \frac{T_e [eV]}{B [Tesla]} > 0 \qquad (39)$$

It is clear that the real part of the frequency of universal drift waves depends on the wavevector in the poloidal plane (k_y) and the electron drift frequency.

The measured frequency shift of the scattered radiation could be explained by these universal drift waves.
The 2 mm scattering apparatus can measure the frequency shift of the scattered radiation at different k vectors. Also various positions in the plasma column can be examined.
So the origin of the density fluctuations can be studied in more detail.

Chapter 3: Experimental set-up

The one channel collective scattering apparatus TURBO, which will be used to study the density fluctuations in TORTUR, is designed to investigate large angle scattering of 2 mm waves.
A mixing technique is used to determine the frequency shift of the scattered radiation. The local oscillator, mixed with the scattered beam, is not frequency shifted with respect to the probing beam, this means that the detection technique is homodyne.
The accessibility of the plasma by means of the viewing ports (the most critical truncating elements) mainly determines the experimental set-up and dimensions of the components used.
The theory of chapter 2 is used to adjust the microwave beam to the torus structure. The power loss due to the truncation of the diagnostic ports of TORTUR is minimized. So an optimal signal to noise ratio is achieved.
This chapter first discusses the collective scattering diagnostic port section followed by a describtion of the beam transport and shaping systems. The third section reports on the transmission of the apparatus and TORTUR. Finaly a review of the TURBO set-up will be given.

3.1: The torus section

The TORTUR section developed to study the density fluctuations has three viewing ports. Figure 14 shows the set-up of this section and the dimensions.

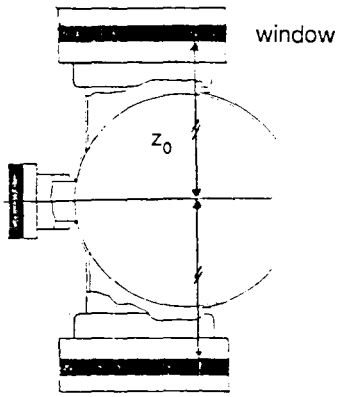

Figure 14: The three viewing ports

The maximum 'foreward' scattering angle is restricted to 50 degrees while the perpendicular scattered radiation can be studied up to an angle of 115 degrees.
Both incident and scattered beam are truncated at the window positions. Therefore a waist of the incident microwave beam positioned at the midplane of the torus gives the optimal transmissivity of the section when the Gaussian beam properties are taken into consideration.

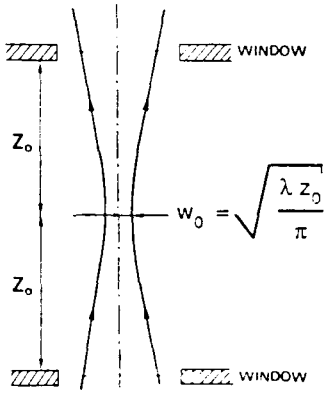

Figure 15: A Gaussian beam in the torus.

In chapter 2 Eq. (14) has been derived, giving the optimal beam radius at the truncating elements. Knowing the distance of the midplane to the windows (146 mm.) one finds the following preferable beam conditons:

radius of the waist (w_0):	10 mm.
radius of the beam at the truncating element (w_{opt}):	14 mm.
divergence angle:	3.8 °

3.2: Beam transport and shaping

The source of the microwave beam is a Varian 140 GHz reflex klystron; it produces 2.14 mm radiation with a maximum power output of 75 mW. The klystron is connected to a oversized waveguide system by means of tapers. Oversized waveguides are used because they transport microwaves without large power losses. The total number of modes that can propagate in an oversized waveguide depends on the dimensions of the cross section of the waveguide compared to the wavelength.
The klystron and the mixer are coupled to fundamental waveguides

and tapers. The higher order modes that can propagate in the oversized waveguides can not propagate in the fundamental waveguides (which acts a mode filter). At irregularities in the oversized wave-
guides a part of the fundamental mode can be converted to higher order modes of propagation of the radiation. These irregularities may excist at the connections of the oversized waveguides to the tapers and the other oversized waveguides. So the amount of connections must be minimized.
Launching antennas, designed to transform the wave into a beam with a Gaussian transverse amplitude variation, 'connect' the oversized waveguides to free space.
Teflon lenses and mirrors are used to shape the Gaussian beam to the beam properties which give the optimal transmission of the torus (see previous section).
A methode is developed to determine the lens position behind the launching antenna and focal length to yield the desired beam divergence angle, waist position and waist radius.

A: A recieving horn antenna, coupled to a crystal detector, is used to measure the transverse intensity profiles of the Gaussian beam. This antenna can be moved along the axis of propagation of the wave and in two directions perpendicular to it. So the horizontal and vertical profiles at various distances from the launching can be measured.

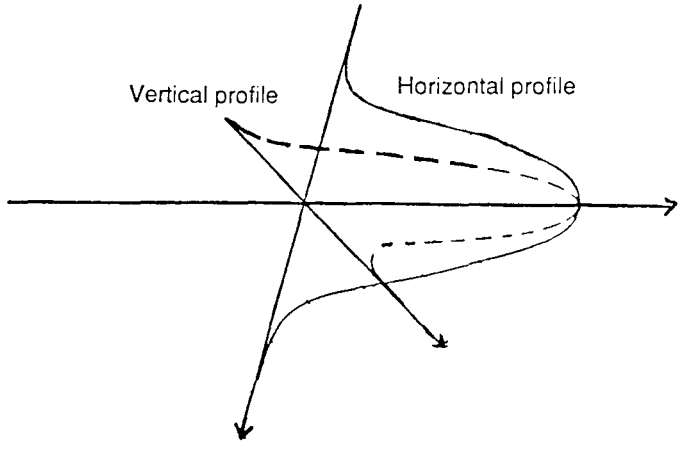

Figure 16: Beam profiles

The radius of the beam, which is defined as the half width of the E-field profile, as a function of the distance from the launching antenna can be determined.

Using

$$w(z') = \sqrt{w_0^2 + \left(\frac{\lambda z'}{\pi w_0}\right)^2} \qquad (5)$$

The radius of the waist (w_0) and the postion of the waist ($z'=0$) of the beam behind the launching antenna can be calculated. The positoin of the waist will be close to the end of the antenna.

B: The desired beam properties behind the lens are known (see previous section). The focal length of the lens can be calculated with the use of the following expression:

$$\frac{1}{w_{waist}^2} = \frac{1}{w_0^2}\left(1 - \frac{z_{lens}}{f}\right)^2 + \frac{1}{f^2}\left(\frac{\pi w_0}{\lambda}\right)^2 \qquad (9)$$

w_{waist} must be 10 mm. z_{lens} = distance of the lens to the calculated waist position.

C: The recieving horn antenna is now used to measure the intensity profiles behind the lens.
If the radius of the waist and the divergence angle match the optimal ones (w_{waist}=10 mm, and a divergence angle of 3.8°) the lens is accepted.
However, if this is not the case the calculated w_0 and the position of the waist do not give the right focal length. This is possible when the profiles before the lens differ from the Gausian intensity distribution. The new radius of the waist behind the launching antenna and its position can be calculated using

$$\frac{1}{w_0^2} = \frac{1}{w_{waist}^2}\left(1 - \frac{z'_{lens}}{f}\right)^2 + \frac{1}{f^2}\left(\frac{\pi w_{waist}}{\lambda}\right)^2 \qquad (9')$$

and

$$z_{lens} = f - \frac{(z'_{lens} - f)\, f^2}{((z'_{lens} - f)^2 + (\frac{\pi w_{waist}^2}{\lambda})^2)} \qquad (10')$$

z'_{lens}: The distance of the waist behind the lens to the lens.
f : The focal length of the lens.
z_{lens} : The distance of the waist behind the launching antenna to the lens.

A new focal length can now be calculated (procedure B; input w_0 and z_{lens} of procedure C).

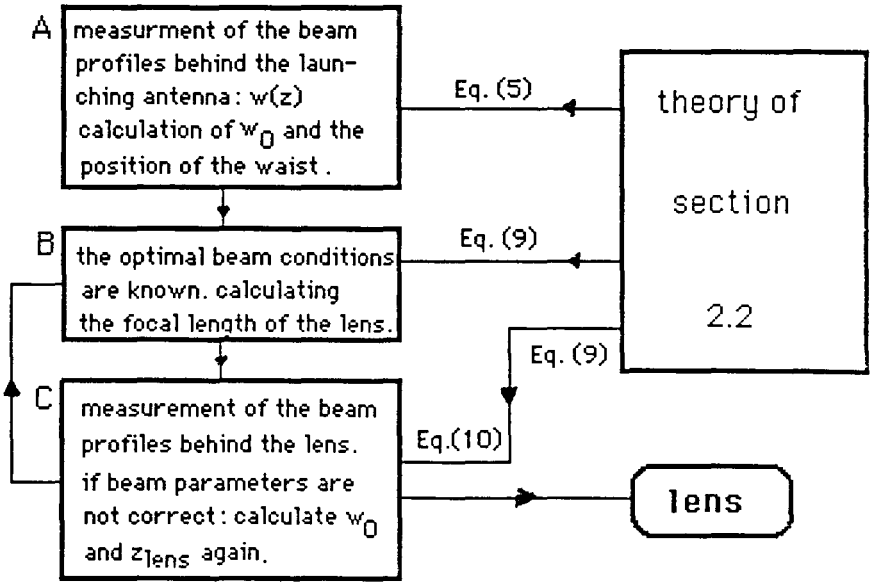

Figure 17: A flow chard of the method used to select a focal length of a lens behind the launching antenna.

Results of the method

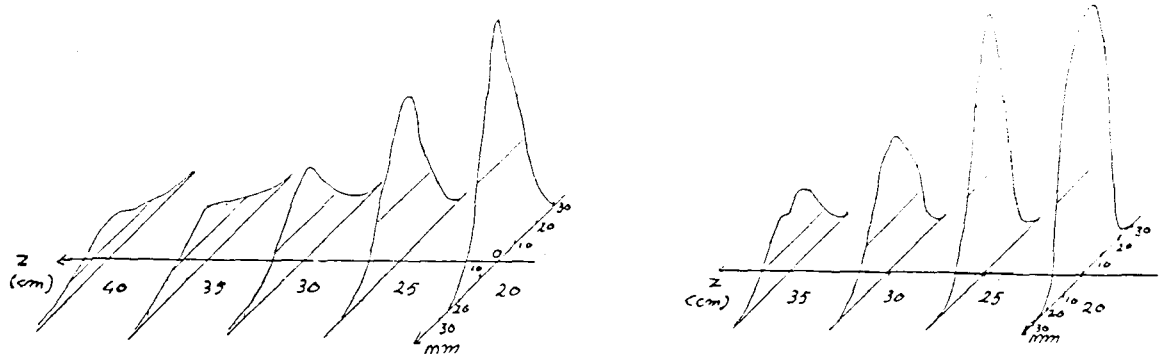

Horizontal profiles

Vertical profiles

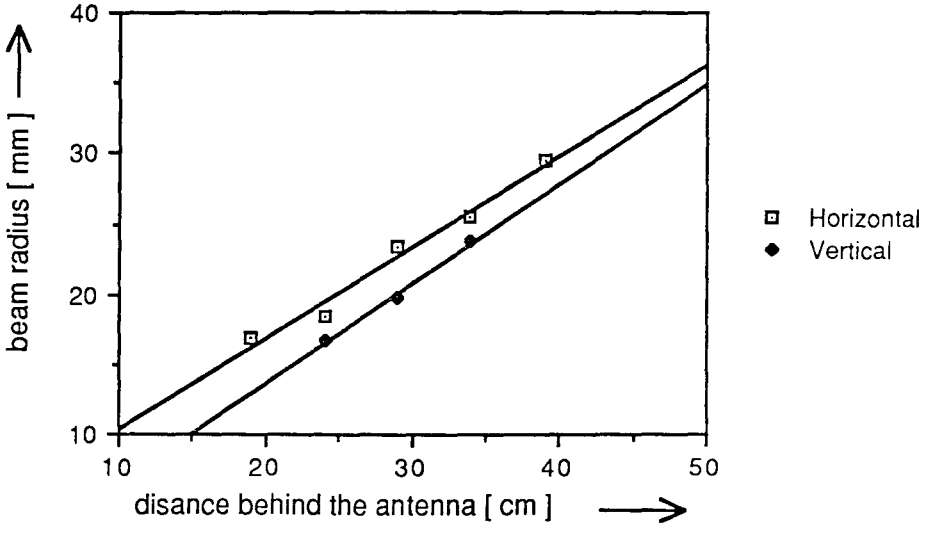

Figure 18 a: The horizontal and vertical intensity profiles behind the launching antenna. b: The beam radius as a function of the distance from the antenna.

The diameter of the lens(es) used to focus the microwave beam is limited to 60 mm giving the possibilty to place the lens(es) between the toroidal field coils. This could be necessary to fulfil the optimal transmission condition of the torus.
Figure 18 shows that the profiles have a Gaussian shape at a distance between 25 cm. and 30 cm. from the launching antenna. The lens will be positioned here.
The calculated radius of the wiast and the position of the waist (procedure A) give an optimal focal length of the lens of 20 cm (procedure B). However, the measurements of the horizontal and

vertical intensity profiles behind the lens showed that the beam properties did not match the optimal ones. So this lens is not accepted and w_0 and z_{lens} are determined again (procedure C). A new focal length is calculated. This optimal focal length, the position of the lens, and the beam properties behind this new lens are:

Optimal focal length of the lens	24 cm.
Optimal lens position behind the antenna:	28 cm.
Horizontal waist radius behind the lens:	11 ± 1 mm.
Horizontal waist position behind the lens:	34 ± 1 cm.
Vertical waist radius behind the lens:	8 ± 2 mm.
Vertical waist position behind the lens:	26 ± 2 cm.

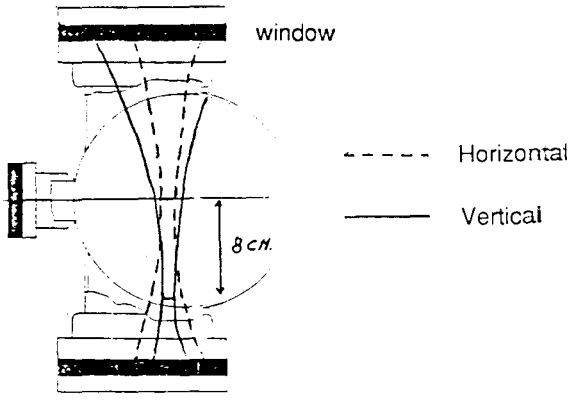

Figure 19: The horizontal and vertical waist position in TORTUR.

The differences between the horizontal and vertical beam properties could not be accepted, because the radius of the vertical was too large at the window above the midplane (see figure) and its divergence angle was not 3.8°. So an correcting lens has to adjust the vertical profile. This lens is cilindricaly shaped and is placed between the other lens and the launching antenna. The focal length could be calculated with the available beam parameters (the radius of the waist, behind the antenna, and the position of the waist calculated at procedure C), yielding - 65 cm. The lens system gives the following beam properties behind it.

Optimal corrigating lens position:	22 cm.
Horizontal waist position:	34 ± 1 cm.
Horizontal waist radius:	11 ± 1 mm.

Vertical waist position:	33 ± 2 cm.
Vertical waist radius:	10 ± 1 mm.
Horizontal beam divergence angle:	3.6 ± 0.4 °
Vertical beam divergence angle:	3.9 ± 0.4 °

It is obvious that the beam behind the lens system fulfils the optimal transmissivity condition of the TORTUR device.
High reflecting gold coated mirrors were designed to vary the foreward scattering angle within the range limited by the torus structure. Two of these mirors are used to inject the probing beam into the plasma and to recieve the scattered radiation at a certain angle.
The recieving branch has the same lens system, oversized antennas and waveguides as the branch of the incident beam throug which the beam is launched, thus giving identical optical paths for both scattered and incident beam.

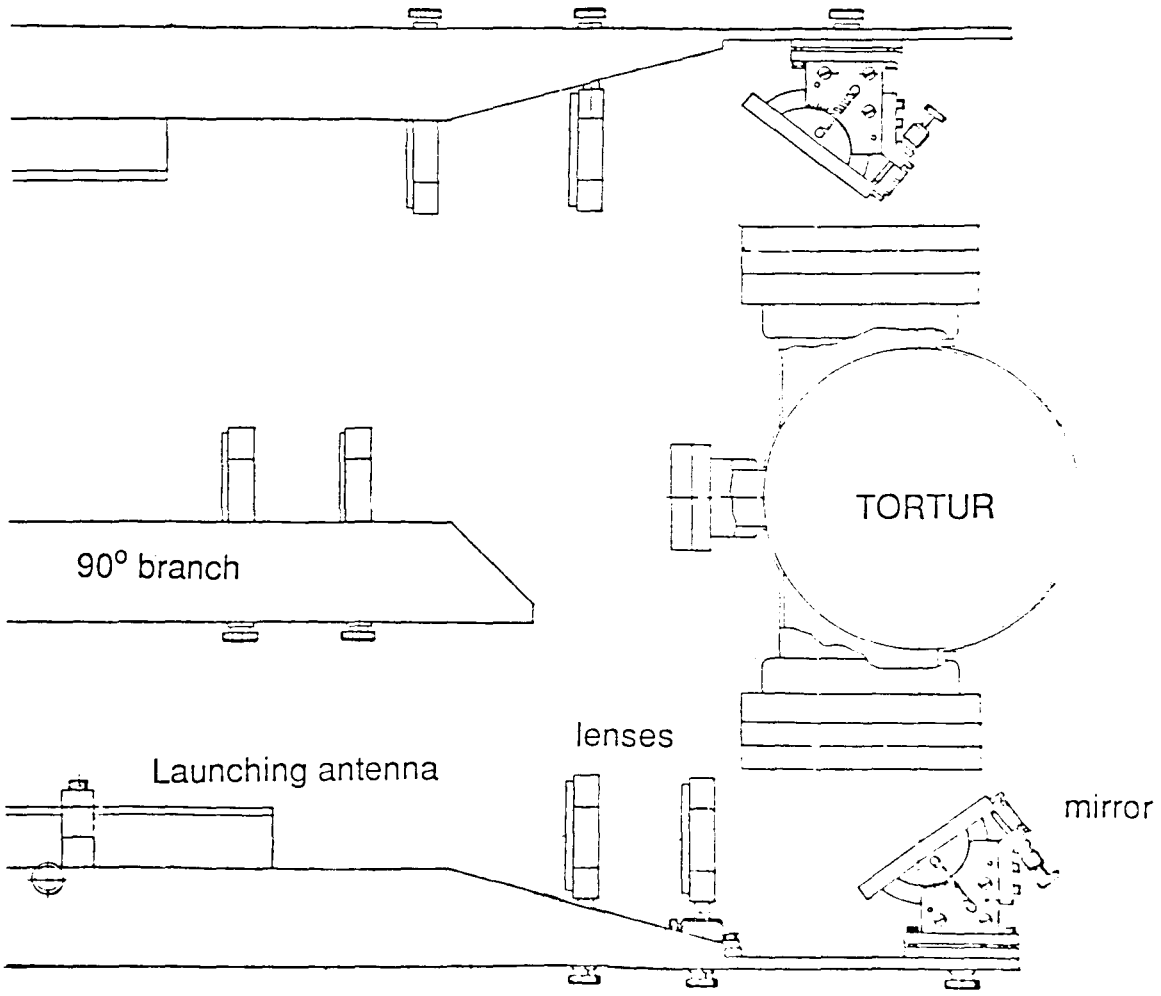

Figure 20: The free space part of the optical path of the microwave beam.

The local oscillator branch:

A beamsplitter in the oversized waveguide branches off a part of the source power for the local oscillator.
The mixer can only be coupled to the local oscillator by means of a fundamental wave guide. A taper is used to connect the beam splitter to a fundamental waveguide transport system.
The following components are included to this transport system:
- a rotational attenuator.
- a hybrid tee.

The attenuator makes it posible to alter the local oscillator power which is fed to the mixer. A bolometer, coupled to the hybrid tee, is used to monitor the local oscillator power.

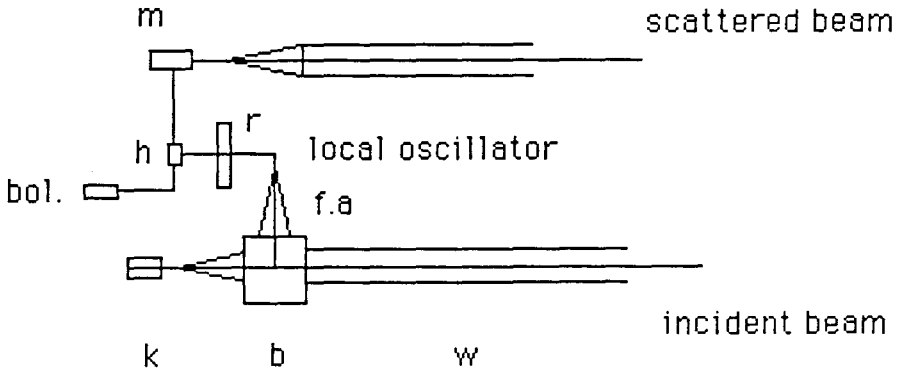

k: klystron
b: beamsplitter
w: oversized waveguide
f.a: taper; oversized to fundamental
r: rotational attenuator
h: hybrid tee
m: mixer
bol.:bolometer

Figure 21: The connection of the local oscillator and the recieving branch to the mixer.

3.3 Transmission of the apparatus

The purpose of the scattering experiment is to measure the frequency shift of the scattered radiation and the absolute fluctuation level of the microturbulence given by

$$\langle \tilde{n}^2 \rangle_{UT} = \beta \sum_i \frac{k_i^2 \langle i_{k_i}(t) \rangle}{4\pi^{5/2} \lambda_0^2 \left(\frac{d\sigma_T}{d\Omega}\right) P_0 P_{lo}} \frac{\sin^2 \theta_{s_i}}{\sin\left(\frac{\theta_{s_i}}{2}\right)} \left(\frac{\hbar \omega_0}{e\eta}\right)^2 \qquad (29)$$

The only unknown quantities in this equation are P_0 (power of the incident beam at the plasma center) and P_{lo}. Therefore it is necessary to measure the loss of power by the various components used in the branch of the incident beam, the recieving branch, and the local oscillator branch. This power loss will be expressed as a transmission factor which is defined as

$$T \equiv \left(\frac{\text{Power output}}{\text{Power input}}\right)_{\text{component}} < 1 \qquad (40)$$

and a attenuation factor

$$A = 10 \log\left(\frac{1}{T}\right) \quad [\text{dB}] \qquad (41)$$

The following tables present the power loss of the various elements and the different transporting branches as a whole

Table 4: Transmision and attenuation

Element	Cause of power loss	Transmission & Attenuation
Taper: fundamental to oversized	mode conversion and absorption	T = 0.89 A = 0.51 dB.
Taper: oversized to free space	mode conversion and absorption	T = 0.91 A = 0.46 dB.
Waveguide: fundamental	absorption	T = $(0.1)^{\text{length [m]}}$ A = 10 dB/m

Waveguide: over-sized	absorption and mode conversion	$T = 0.96^{\text{length [m]}}$ A = 0.2 dB/m
Beamsplitter	branching off the power in two directions (0° and 90°)	$T_0 = 0.62$ $A_0 = 2.1$ dB. $T_{90} = 0.43$ $A_{90} = 3.7$ dB.
Hybrid tee (fundamental)	branching off the beam in three different directions, absorption	one direction T = 0.25 (3 times) A = 6.0 dB.
Lenses	truncation, reflection and absorption	T = 0.83 A = 0.8 dB.
Mirrors	disturbance by irregularities of the surface.	T = 0.995 A = 0.02 dB.
Attenuator	Rotation of fundamental waveguide	T = 1 - 0.001 A = 0 - 30 dB.

The local oscillator branch consists of

1 taper oversized to fundamental.
10 cm fundamental waveguide.
1 rotational attenuator.
1 hybrid tee.

It has a variable transmission factor.

The branch of the incident beam consists of

1 taper oversized to free space.
4 cm. fundamental waveguide.
1.5 m. oversized waveguide.
2 lenses (the lens system).
1 gold coated mirror.

Transmission factor T = 0.53.

The recieving branch has the same components as the plasma branch and a taper fundamental to oversized giving T = 0.47.

Since the transmission factors of the branches are known the local oscillator power can be calculated, but the power in the plasma center remains unknown because the transmission of the TORTUR device has not been determined jet.

Transmission through TORTUR:

The three viewing windows in the TORTUR collective scattering section absorb some of the power in the beam. The dimensions of the port entrance cause also some power loss by means of truncation of the microwave beam. So the the foreward scattered radiation and the incident beam must pass at least one window which acts as a truncating element and absorbs some of the power. The truncation factor (transmissivity) can be calculated,using Eq (13), yielding T = 0.94.
The measurement of the window absorption (transmission) is not possible in a direct way because TORTUR could not be opened. The following method is used to determine the transmission factor.

I: An exact copy of the diagnostic windows, placed in the microwave beam between the two mirrors, is irradiated under several angles by turning the window, thus giving the transmission as a function of the angle of incidence with respect to the normal vector (see figure).

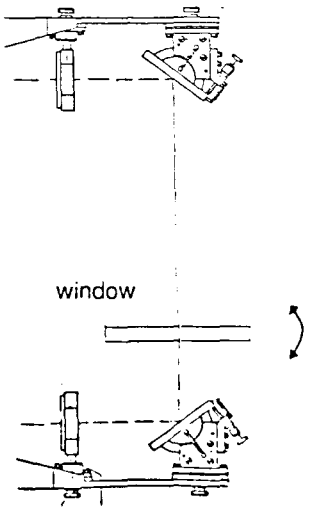

Figure 22: Transmission measurement set-up.

II: The TORTUR section as a whole can not be rotated, so the mirrors are used to accomplish the required variation in angle. Because of the torus structure the angle can only be variated between 0° and 10° (see figure 23). The transmision of the section is measured.

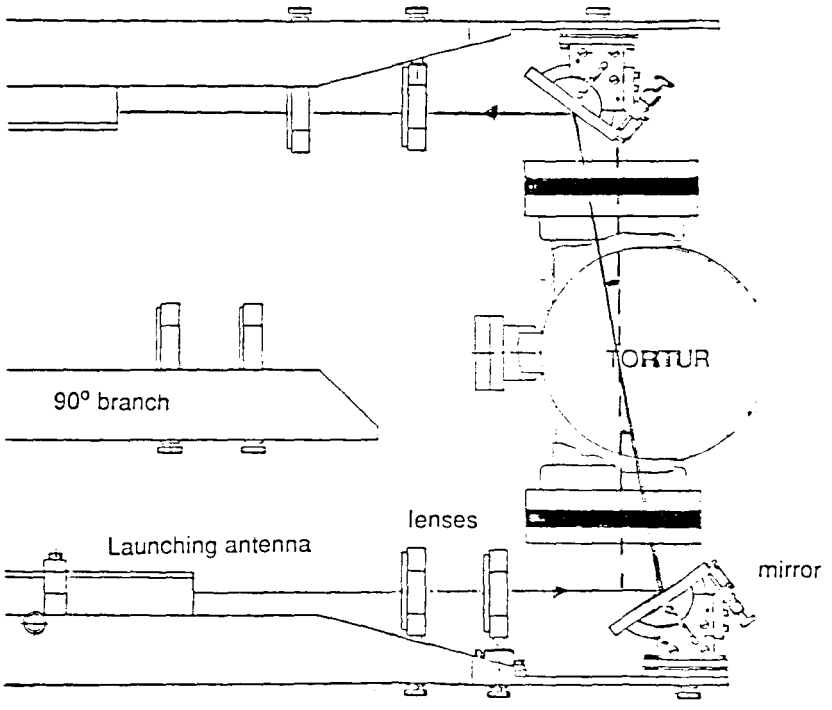

Figure 23: TORTUR transmission measurement set-up.

The windows absorb and truncate the beam. Assuming the two windows are identical and knowing the truncation of the entrance slit, the transmission of a single torus window can be calculated.

The slope of the transmission factor is given by I and the absolute value of it are by II. However the absolute values can only be measured up to an angle of 10 degrees. By combining the two results (I and II) the absolute transmission factors of a TORTUR window can be determined.

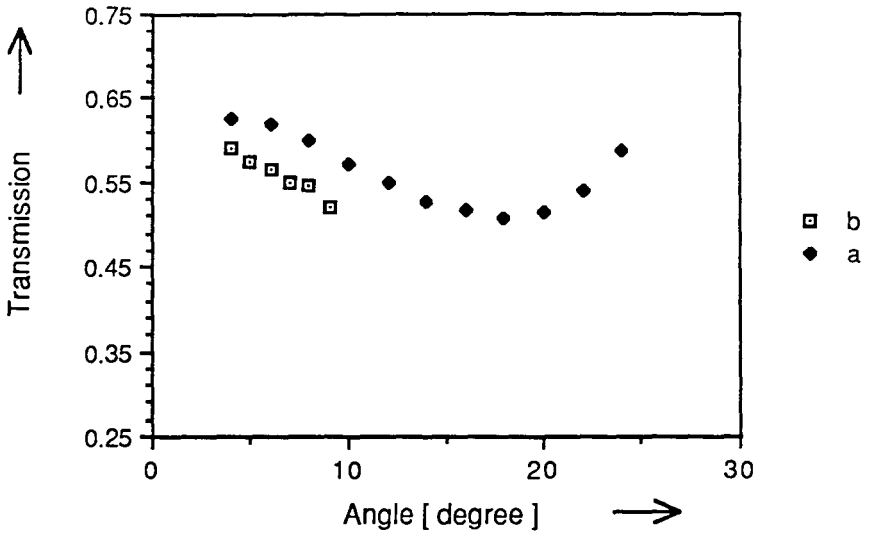

Figure 24 a: The tranmission of the spare window (I).
b: The transmission of a TORTUR window (II)

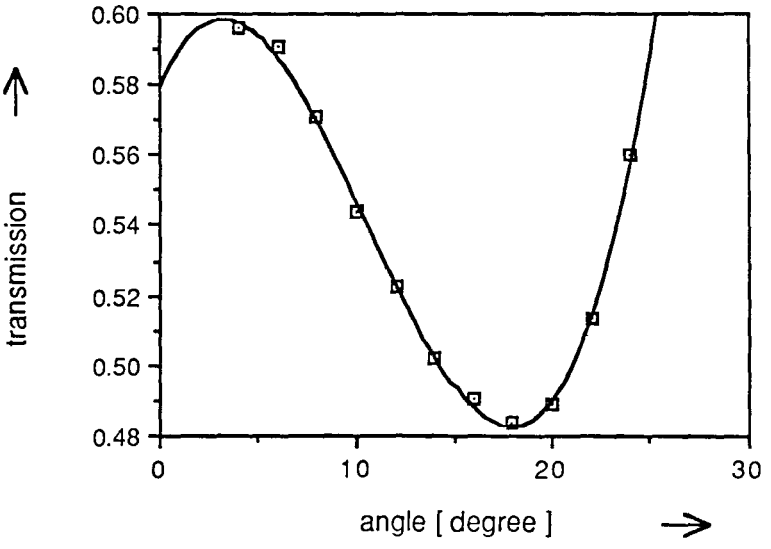

Figure 25: The transmission of a TORTUR window versus the angle of incidence.

3.4 Beam reflection problems

The microwave is tranported in free space by lenses and mirrors and is coupled to the oversized waveguides by horn antennas. The

surfaces of these elements may reflect the microwave beam. This causes an standing wave pattern between the antennas. A demonstration of the excistence of such a pattern follows from the beam profile measurements at a certain distance from the launching antenna.
The amplitude variation of the profile maximum, measured with a cristal detector coupled to a recieving horn antenna, along the axis of propagation is shown in figure 26.

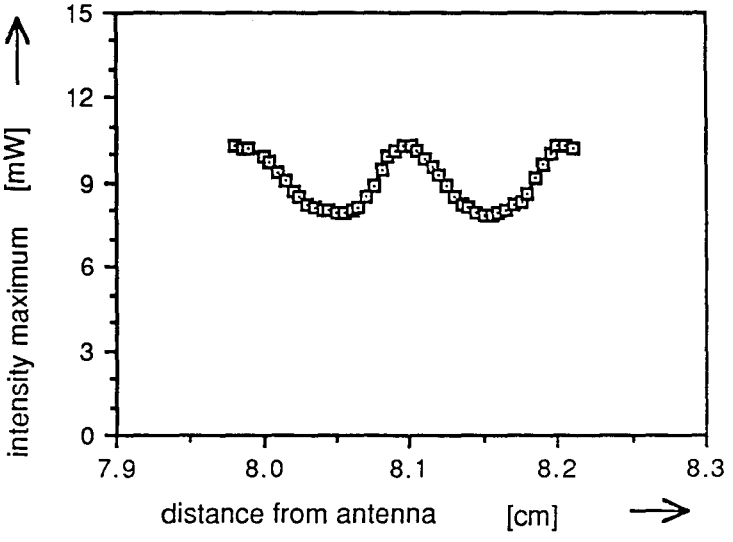

Figure 26: A standing wave pattern between two horn antennas.

A standing wave pattern may be caused by the element of which the transmission is measured. The transmission of the lenses and the diagnostic ports of TORTUR is not calculated according equation (40). The power of the beam before the element could not be measured, instead of this the power when the element is not placed in the beam is used. The transmision defined in eq (40) can not be influenced by the standing wave pattern. The differently calculated transmission of the lenses and the torus section can vary due to the standing wave.
Changing transmissiion factors appear in the following circumstances.

* By changing the possition of the lenses the transmission factors of the branch of the incident beam and recieving branch vary appreciably even if the positions are sligthly changed. Equation

(36) shows that the transmision factor of the branches influences the signal to noise ratio of the scattered signal. So the four lenses must be positioned with great care.

* The results of the measurements of the transmision of the window at angles of incidence below 4 degrees demonstrate a large variation of the transmission factor at the same conditions. The reflection of the beam at the surface of the window enhances the standing wave pattern so even the smallest window position variation changes the transmission factor. In order to avoid this the angle of incidence can not be chosen below 5 degrees.

The problems due to the standing wave pattern are enhanced by the compact set-up of the apparatus (all the elements used in the free space part of the optical path are placed within 1.3 meters).

3.5 Review on the TURBO apparatus

The collective scattering apparatus TURBO has the following characteristics.

P_0 = 11 mW
P_{lo} = 0 - 6 mW
P_{source} = 65 mW

Transmission of the branch of the incident beam	= 0.53
Transmission of the recieving branch	= 0.47
Transmision of the local oscillator branch	: variable

When the observed volume is placed at the plasma centre the following scattering angles can be used:

Foreward scattering angles: 5° to 50°
Perpendicular scattering angles: 90° to 115°

wavenumber resolution

$\Delta|\underline{k}| = \Delta k_x \approx 2\ cm^{-1}$

The minimum fluctuation level we want to detect is:

The minimum fluctuation level we want to detect is:

$$\frac{\tilde{n}}{n_e} = 10^{-5}$$

The signal to noise ratio N of the scattered signal at this minimum fluctuation level can be calculated with the use of

$$P_{source} = \frac{1}{T_{br}} \left\{ \frac{P_{lo}}{T_{lo}} + \frac{0.76\ N}{\lambda_0\ P_{lo}\ T_{pl}^2} \left[1 + \frac{L\ T_{pl}\ P_{lo}\ \lambda_0^2\ I_{ece}}{NEP\ 10^9} \right] \right\} \qquad (36)$$

The signal to noise ratio is dominated by the total amount of E.C.E light near the second harminic frequency.

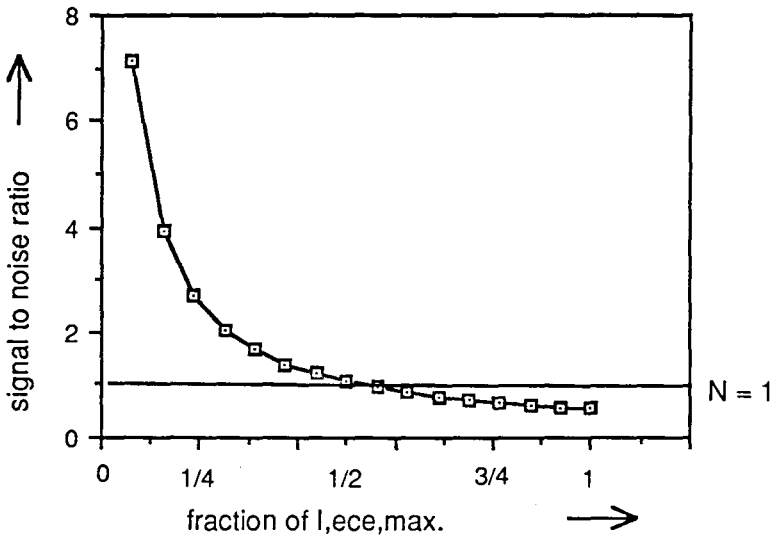

Figure 27: The signal to noise ratio of the scattered signal from the minimum fluctation level as a function of the amount of E.C.E light near the second harmonic frequency.

Chapter 4: The first results

The Alpha mixer produces a current $i_k(t)$. This output signal is amplified (20 dB) by a low noise preamplifier, which has a frequency pass band of 100 MHz, and is fed to a A-D converter (maximum sample frequency; 32 MHz). Two series of 4 kbytes information are recorded for later analysis on a PDP 11/70 computer.
Fast Fourier transform procedures give a power spectrum of the density fluctuations at a certain k-vector ($S_k(\omega)$). This power spectrum relates to the output current of the mixer as follows.

$$S_k(\omega) \sim I_k(\omega)$$

where $I_k(\omega)$ is the Fourier transform of the autocorrelation of $i_k(t)$. From the power spectra the characteristics of the density fluctuations are deduced.

The observed volume was placed near the centre of the plasma (at r= 1 cm).
The measurements were done during the plateau stage of the discharge (one plasma shot gives one measurement). The plasma current at the plateau stage was equal to 30 kA (see figure 2) and the loop voltage was equal to 5 V (high loop voltage discharge).
Only the loop-voltage, plasma current, and position of the plasma column were determined. The diagnostics to measure the electron density and electron temperature could not be used.

4.1: The output signal of the mixer.

The noise NEP*B and the electron cyclotron emission near the second harmonic frequency (see section 2.3) contribute to the output signal of the mixer, wich is digitized with sample frequencies of 4 MHz and 8 MHz by the A-D converter.
The contribution of the noise factors to the output signal is measured.

- The mirrors of the scattering apparatus are removed. So the microwave beam is not injected into the plasma and no plasma light is recieved. The local oscillator power is 5 mW.
  The output signal is a result of the noise of the mixer.
  The measurements showed that the contribution of this noise factor to the output power of the mixer can be neglected.

- One mirror is used to measure the E.C.E noise. The 'incident' beam is not injected into the plasma.
  The amplified signal of the mixer has a maximum variation of 12 mV (the total range of the ADC is 512 mV, sensitivity: 2 mV/bit).

The total output signal of the mixer in the A-D converter at a scattering angle of 10^{o} is shown in figure 28. It exceeds the total contribution of the noise factors. The wavenumber of the scattered radiation which has been investigated at this scattering angle equals 5 cm^{-1}.

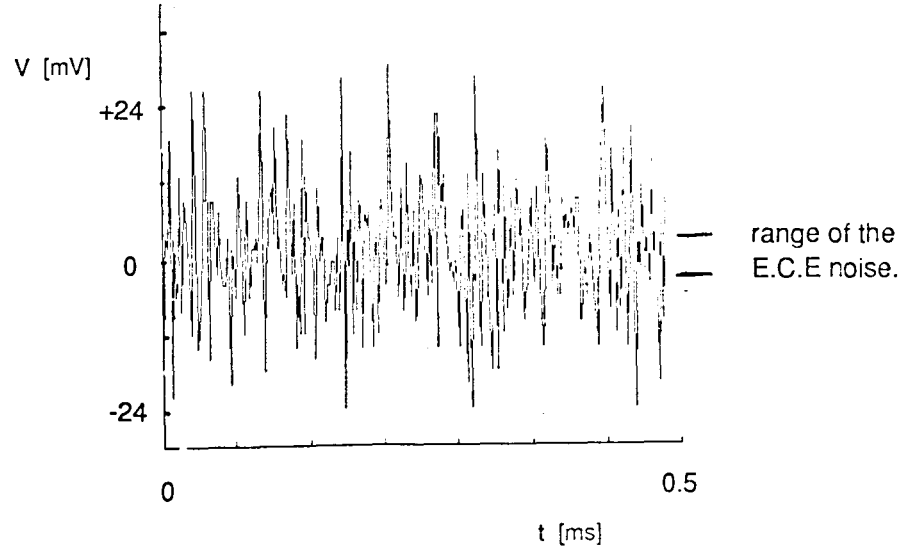

Figure 28: The time development of the total output signal of the mixer recorded by the A-D converter.

4.2: The power spectrum at one scattering angle.

The total recording time of the ADC can be devided in various intervals in time. The starting time of these intervals can be freely chosen. The minimum length of the interval is restricted by

the fast Fourier procedure. Below a certian number of data points (<100) the Fourier transform is not reliable.
The power spectra at different intervals within the recording time are given in figure 29.
The amplitude of the spectrum and the position of the frequency spikes vary in time . So only the range of the frequency shift at a certain k value can be determined.

The variation of the scattered signal becomes clear when the power spectrum is determined at the smallest possible (reliable) length of the time interval (Δt_m), and is integrated over a frequency range Δf. This frequency intergrated spectrum is called S_k. Figure 30 shows the time development (Δt_m= 25 μs) of S_k at four different intervals of the total range of the frequency shift.
From these resuls can be deduced that some 'events' take places within 25 μs. The power spectrum integrated over the frequency range of 500 kHz to 1 MHz suggest a periodical behaviour with a characteristic time of a few hundred microseconds. However, further investigation of these phenomena is necessary.

4.3 Power spectra at four different scattering angles.

The phase and group velocity of the instabilies can be determined from shift in position of the frequency spikes of the power spectrum as a function of the investigated k value [3].
The power spectra at four different scattering angles (10°,15°, 20°, and 35°) are analysed.
The power spectra at these scattering angles are given in figure 31. It is obvious that the amplitude of the power spectrum decreases at larger k values. The position of the frequency spikes at the investigated k values vary in time (see also previous section). Only the frequency range of the position of the spikes can be given. So no group or phase velocity can be determined.
The power spectrum averaged in time is calculated by taking the length of the interval in time as long as possible (1/3 of the recording time). The power spectra are smoothed.
Besides the decrease in magnitude at larger scattering angles these single humped spectra do not relate to the investigated k value (see figure 32).

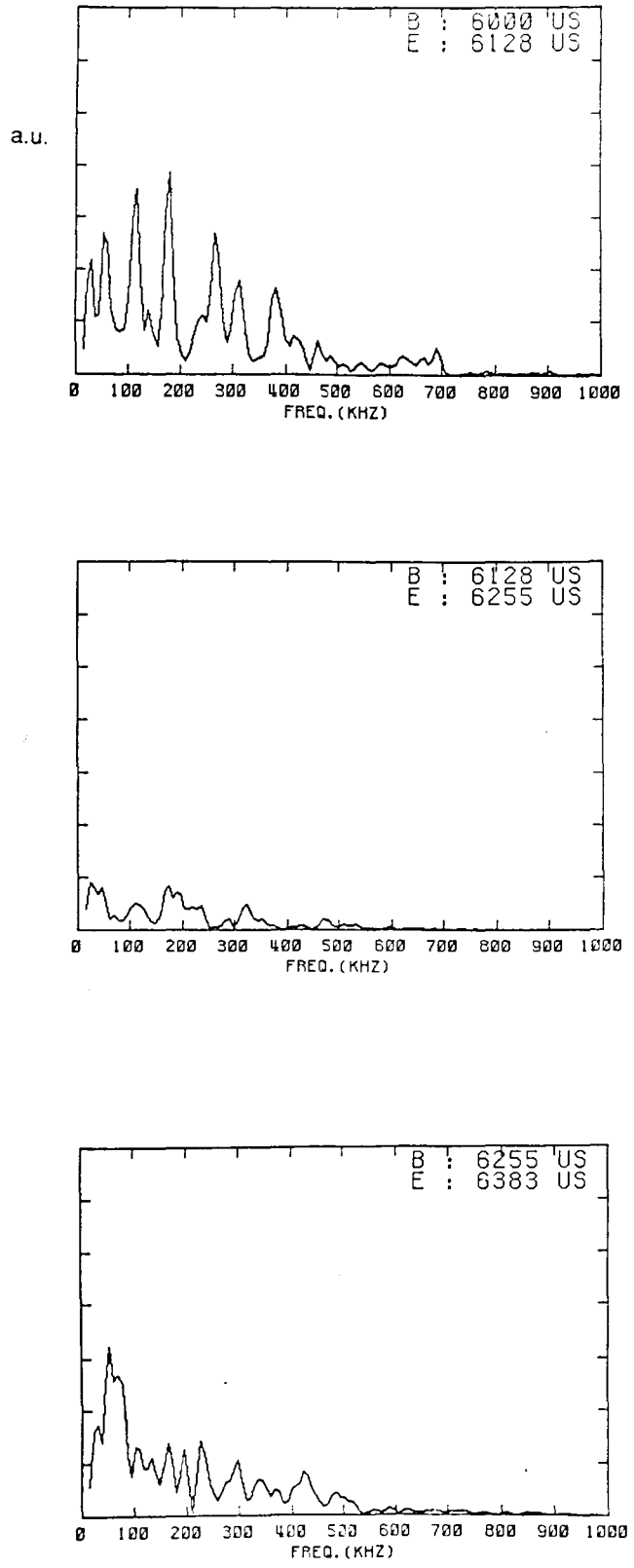

Figure 29: The power spectrum at k = 5 cm $^{-1}$ at different time intervals within the recording time of the A-D converter.

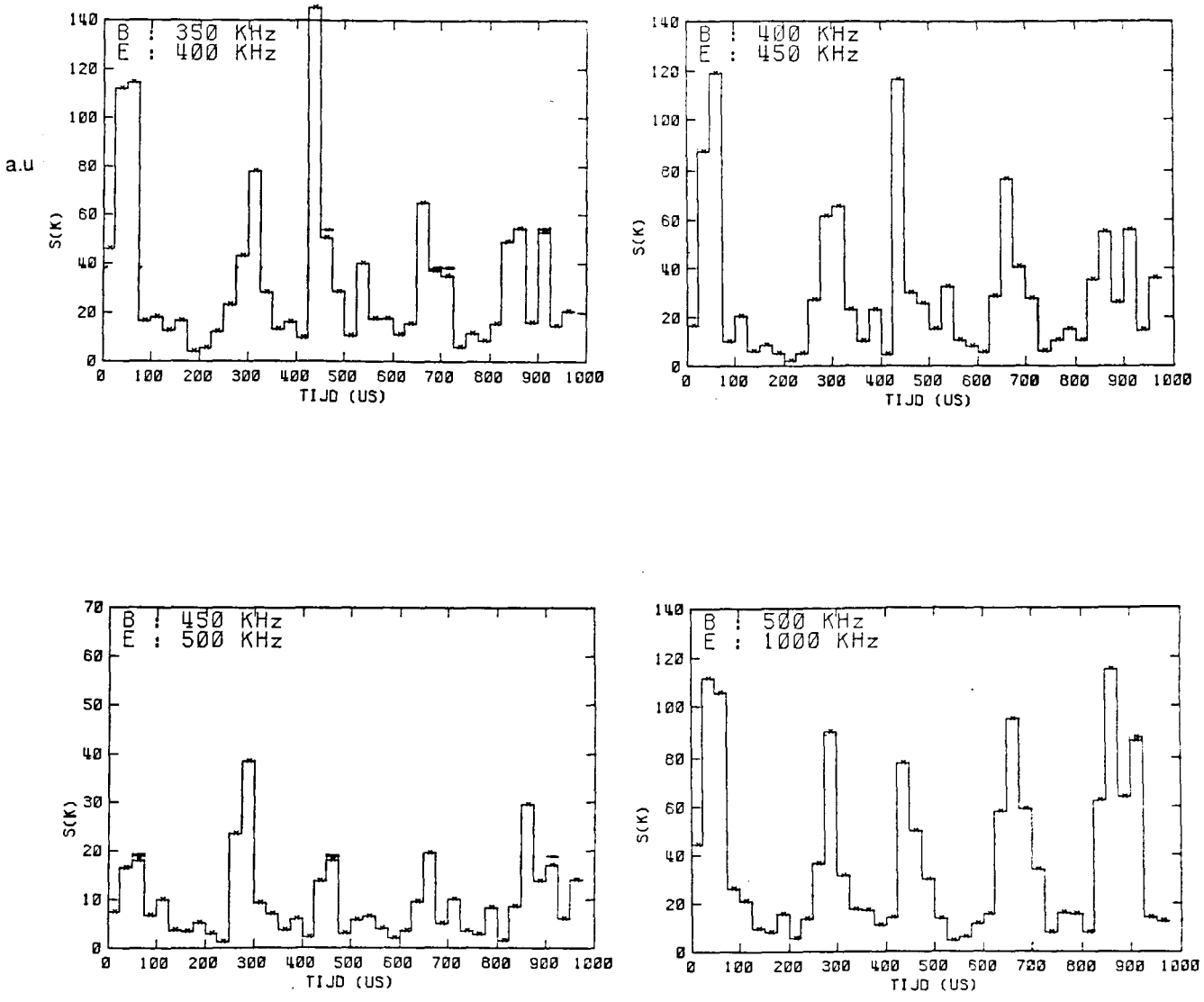

Figure 30: The power spectrum at k = 5 cm $^{-1}$,integrated over four different frequency ranges ,versus time (Δt = 25 μs)

a.u.

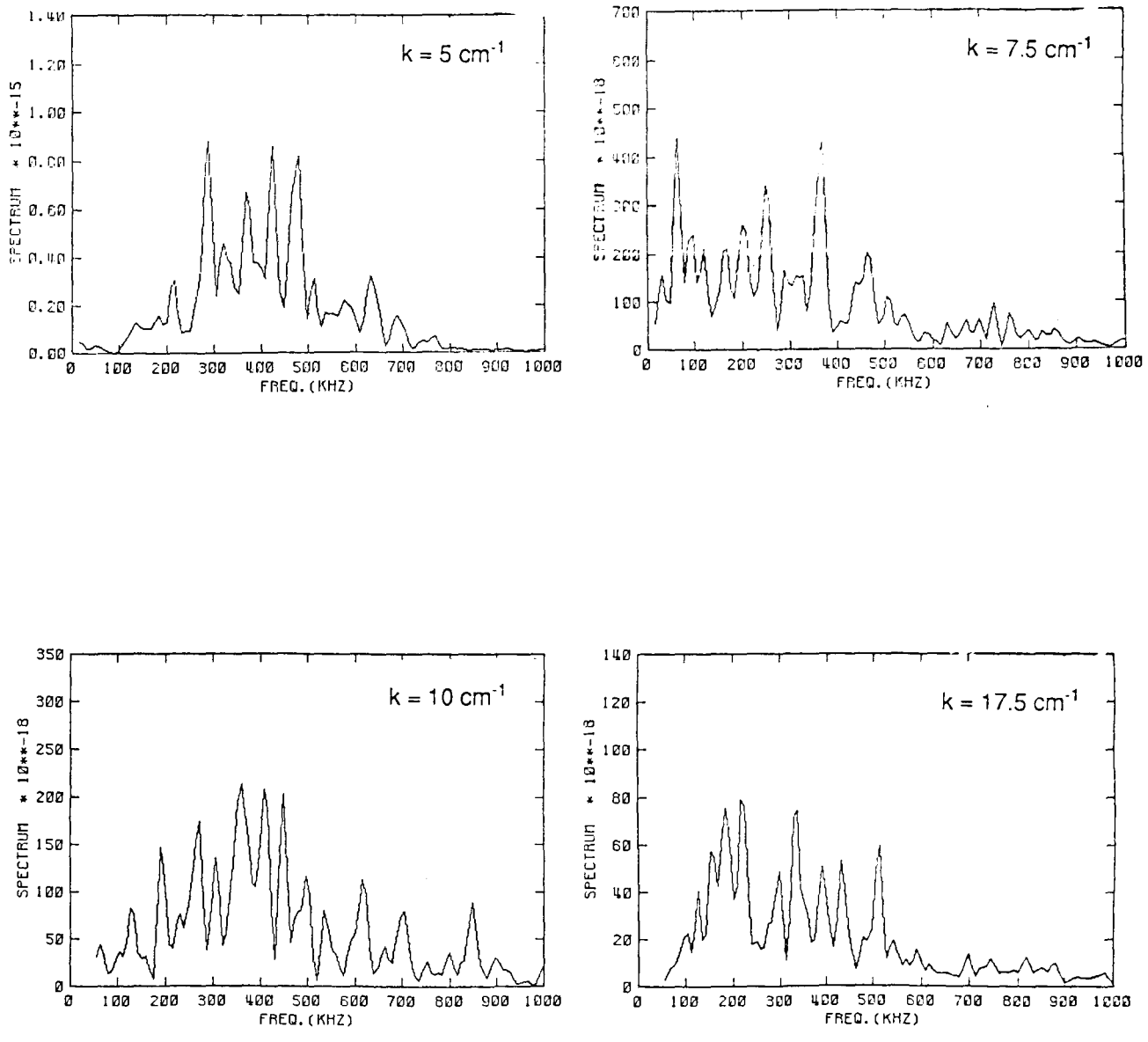

Figure 31: The power spectrum at four different scattering angles (10 °,15 ° ,20 °,and 35 °) . Δt = 128 μs.

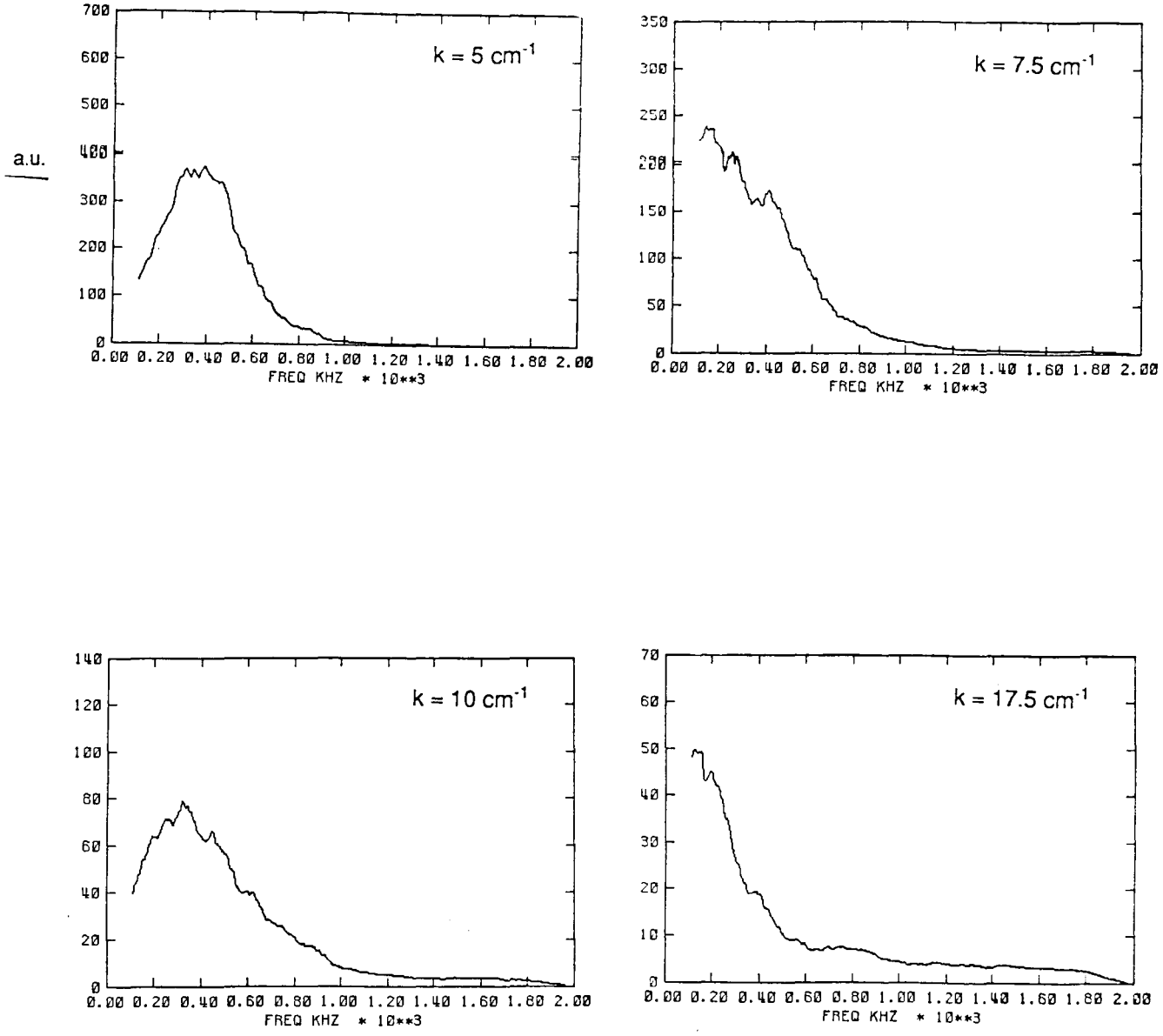

Figure 32: The smoothed power spectra averaged in time.
Δt = (recording time)/3

4.4 Summary

- The scattered signal exceeds the contribution of the noise caused by the E.C.E light.
- The magnitude of the power spectra changes within the recording time of the A-D converter.
- The position of the spikes of the power spectra vary within the recording time.
- S_k shows a rapid change over the entire frequency range (events take place within 25 μs) and a possible periodical behaviour at the higher frequency domains (500 kHz to 1 MHz) of the power of the scattered radiation.
- The magnitude of the power spectra decreases at larger k values of the density fluctuations.
- A phase or group velocity can not be determined.
- The frequency range, where the dominant spikes in the power spectra are situated, does not relate to the investigated k values.

REFERENCES

[1] T.F.R Group and Truc A. (1984) Plasma physics & Controlled fusion 26, 1045.

[2] Evans D.E. (1985) Rev. Sci. Instrum. 56, 902.

[3] Brower D.L., Peebles W.A., Luhman N.C. PPG-1050 march, 1987.

[4] Holzhauer E. (1978) Plasma Phys. 20, 867.

[5] Grésillion D. (1982) Physica Scripta T2/2, 459.

[6] Huussen F., Ikezawa S., de Kluiver H. (1985) Plasma physics & Controlled fusion 27, 447.

[7] de Kluiver H., Barth C.J., Donné A.J.H., I.R. 87/002.

[8] Barth C.J., Rijnhuizen I.R. 85/052.

[9] Remkes G.J.J., Sips A.C.C., Rijnhuizen Report 87-172, to be published

[10] Sillen R.J.M., Proc 5th. Int. Workshop on ELectron Cyclotron Emission and Electron Clyclotron Resonance Heating, San Diego, 9-11-12 November 1985.

[11] Siegman A.E. (1966) Appl. Opt. 5, 1588.

[12] Sheffield J. (1975) Plasma scattering of electromagnetic radiation, Academic Press, New York, 1975

[13] Miyamoto K., Plasma Physics for Nuclear Fusion, 1976, English translation, MIT Press, Cambridge, 1980.

[14] Button K.J. (1979) Infrared & millim. waves 2, 84, Academic Press, New York, 1979.

[15] Button K.J. (1979) Infrared & millim. waves 6, 278.
Academic Press, New York, 1982.

[16] TORTUR Team, Donné A.J.H., Rijnhuizen I.R. 87/012.

Appendix: Universal drift waves

This appendix analyses a dispersion equation describing the characteristics of universal drift waves. They are induced by a pressure gradient in the plasma. These drift waves have frequencies lower than the ion cyclotron frequency $|\Omega_i|$ and are excited by an inverse electron-Landau damping process.

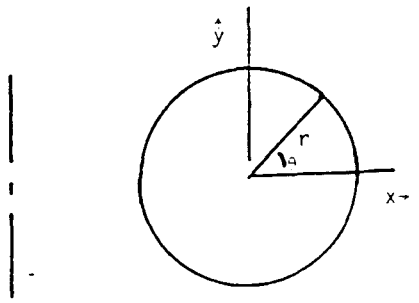

Figure A1: The grid of coordinates.

A density gradient in the plasma is taken along the x axis.
The uniform magnetic field in the direction of the z axis together with a uniform gravitational field $G = Ge_x$, which accounts for the finite radius of curvature of the magnetic field lines, determine the zeroth-order approximation of the particle motion.
By linearizing the quantities used and substituting them in the collisionless Boltzmann equation an expression for the first order pertubation (f_1) of the distribution function is found.
A plane wave approximation simplifies the calculation of the f_1 which can than be used in the following dispersion equation.

$$\Delta\phi = \frac{1}{\varepsilon_0} \sum_J q_J \int f_{1J}\, d\underline{v} \qquad (A1)$$

where $\phi(\underline{r}, t) = \phi(x) \exp(i k_y y + i k_z z - i\omega t)$ (A2)

The subscript j denotes the particle type (ion, electron).
Complicated integration over the velocity space with the use of

the zeroth-order distribution function gives the dispersion equation for electrostatic instabilities.
The Maxwellian distribution function includes the x coordinate dependence of the density.

$$f_0 (v_\perp^2 - 2Gx , v_z^2 , x - \frac{v_y}{\Omega}) = n (x - \frac{v_y}{\Omega}) (\frac{m}{2 \pi T_\perp}) \sqrt{\frac{m}{2 \pi T_z}} \exp (- \frac{m}{2 T_\perp} (v_\perp^2 - 2Gx) - \frac{m}{2 T_z} v_z^2) \qquad (A3)$$

where $G = \frac{(T_\perp + T_z)}{m R}$

R = Radius of curvature of the magnetic force lines.

T_z = Temperature in eV paralel to the magnetic field.

$T_\perp$ = Temperature in eV perpendicular to the magnetic field.

$\Omega = - q B / m.$

$v_\perp = v_x^2 + v_y^2$: Particle velocity perpendicular to the magnetic field.

Assuming a isotropic hydrogen plasma ($T_\perp = T_z$, Z=1) without temperature gradients and plasma current the dispersion equation describing low frequency drift waves is

$$0 = (k_y^2 + k_z^2) \frac{\varepsilon_0 T_e}{n q^2} + \frac{T_e}{T_i} (1 + \exp (- b_i) I_0 (b_i) \xi_{i0} Z (\xi_{i0}) (1 - \frac{\omega_i^*}{\omega_{0i}})) + (1 + \exp (- b_e) I_o (b_e) \xi_{e0} Z (\xi_{e0}) (1 - \frac{\omega_e^*}{\omega_{0e}})) \qquad (A4)$$

with $b_i = (k_y \rho_i)^2$ and $b_e = (k_y \rho_e)^2$

ρ_i = Ion Larmor radius.

ρ_e= Electron Larmor radius.

I_0 = Modified Besselfunction.

ω_i^* and ω_e^* are the drift frequencies of the ions and electrons respectivily. They are defined as

$$\omega_i^* \equiv - k_y \, [m^{-1}] \left(\frac{1}{n}\frac{dn}{dx}\right) \frac{T_i [eV]}{B [Tesla]} < 0 \qquad (A5)$$

$$\omega_e^* \equiv k_y \, [m^{-1}] \left(\frac{1}{n}\frac{dn}{dx}\right) \frac{T_e [eV]}{B [Tesla]} > 0 \qquad (A6)$$

The function $Z(\xi)$ is called the plasma dispersion function and its argument ξ_{j0} relates

$$\xi_{J0} = \frac{\omega_{0J}}{\sqrt{2}\, k_z} \sqrt{\frac{m}{T_J}} \qquad (A7)$$

and $$\omega_{0J} \equiv \omega - \frac{k_y G}{\Omega_J} \qquad (A8)$$

A solution $\omega = \omega_r + i\gamma$ of the dispersion equation for G=0 and zero Larmor radius for the electrons will be

$$\frac{\omega_e^*}{\omega_r} = \frac{\frac{T_e}{T_i}(1 - \exp(-b_i)\, I_0(b_i)) + 1}{\exp(-b_i)\, I_0(b_i)} \qquad (A9)$$

$$\frac{\gamma}{\omega_r} = \sqrt{\pi}\ \frac{k_z}{|k_z|}\left(\frac{\xi_{e0}\exp(-\xi_{e0}^2)\left(1-\frac{\omega_r}{\omega_e^*}\right)}{\exp(-b_i)\,I_0(b_i)} - \right. \qquad \text{(A10)}$$

$$\left. - \xi_{i0}\exp(-\xi_{i0}^2)\left(1+\frac{\omega_r}{\omega_e^*}\frac{T_e}{T_i}\right)\right)$$

where the large argument approximation for $Z(\xi_{i0})$ and the small argument approximation for $Z(\xi_{e0})$ is used.
The second term in the numerator of γ/ω_r is the contribution of ion Landau damping while the first term contributes to instability when $\omega_r/\omega_e^* < 1$.
Universal drift waves are characterized by parallel phase velocities, lying between the ion and electron thermal velocities.

$$\sqrt{\frac{T_i}{m}} < \left|\frac{\omega}{k_z}\right| < \sqrt{\frac{T_e}{m}} \qquad \text{(A11)}$$

The influence of G on the solution depends on the sign of R.
$R > 0$ for concave-outward curvature and $R < 0$ for convex inward curveture of the magnetic force lines ($R > 0$ for a tokamak).
Because

$$\xi_{i0} = \frac{\omega_{0i}}{\sqrt{2}\,k_z}\sqrt{\frac{m_i}{T_i}} = \frac{\omega - \frac{k_y G_i}{\Omega_i}}{\sqrt{2}\,k_z}\sqrt{\frac{m_i}{T_i}} = \frac{\omega + \frac{2k_y T_i}{qBR}}{\sqrt{2}\,k_z}\sqrt{\frac{m_i}{T_i}} \qquad \text{(A12)}$$

and $$\xi_{e0} = \frac{\omega - \frac{2k_y T_e}{qBR}}{\sqrt{2}\,k_z}\sqrt{\frac{m_e}{T_e}} \qquad \text{(A13)}$$

the ion-Landau damping term decreases if $R > 0$ (ξ_{i0} increases) and the first term of the numerator of γ/ω_r will be enhanced.

This can be explained as an reinforcement of the gradient drift by a drift caused by the centrifugal force on the particles.
The frequencies of universal drift waves lie in the 50 kHz to 500 kHz range, depending on the plasma conditions, the k_y vector to be studied and, the position of the observed volume.